Nonlinear Dyn (2019) 96:363–387
https://doi.org/10.1007/s11071-019-04794-0

ORIGINAL PAPER

Observer-based estimation of velocity and tire-road friction coefficient for vehicle control systems

Ying Peng · Jian Chen · Yan Ma

Received: 16 June 2017 / Accepted: 18 January 2019 / Published online: 31 January 2019

Abstract A novel nonlinear observer for the estimation of vehicle velocity together with the tire-road friction coefficient is presented in this paper. The modular observer is designed based on a longitudinal tire force estimation approach and a lateral tire friction model. Compared to the state-of-art methods, the proposed observer design provides accurate estimation of the longitudinal velocity, lateral velocity, and the tire-road friction coefficient simultaneously. Particularly, the longitudinal tire forces are first estimated based on a filter observer. Then, according to the calculation of lateral tire forces, the nonlinear observer is proposed to estimate vehicle velocity and the tire-road friction coefficient. Moreover, the stability property of the observer is analyzed using a Lyapunov-based method. Simulation results validate the effectiveness of the proposed method.

Keywords Vehicle dynamics · Modular observer · Longitudinal velocity · Lateral velocity · Tire-road friction coefficient

This work was supported by the National Natural Science Foundation of China under Grant 61433013.

Y. Peng · J. Chen (✉) · Y. Ma
State Key Laboratory of Industrial Control Technology, College of Control Science and Engineering, Zhejiang University, Hangzhou 310027, China
e-mail: jchen@zju.edu.cn

1 Introduction

Driver assistance systems, e.g., automated highway systems, depends on reliable vehicle control performance [1]. The reliability of vehicle control performance in terms of handling, stability and comfort depends greatly on the precise estimate of vehicle states such as longitudinal velocity, lateral velocity, and the tire-road friction coefficient (TRFC) [2,3]. Based on the estimated parameters, a proper energy efficiency control can be proposed to reduce energy consumption [4]. However, it is hard to measure the vehicle states mentioned above directly because of high cost and low reliability [5]. Hence, to achieve a good control performance, real-time estimation of vehicle states based on the information from some basic low cost vehicular sensors has become popular [6].

The estimation methods for TRFC can be categorized into cause-based and effect-based methods [7]. Cause-based methods focus on the study of detecting influence factors in the interaction of the tire and the road, and then identify the TRFC using certain analytical theories [7]. To our knowledge, three different approaches to identify the TRFC have been tried, including appliance of optical sensors, acoustic sensors, and tire-tread sensors [8–10]. Optical sensors are installed at the front of the vehicle, the reflections from the surface are used to estimate the road surface [8]. This approach has the advantage of being able to estimate the friction slightly before the tires reach, for

instance, an icy spot. However, a difficulty here is keeping the sensors clean. Acoustic sensors can be used to listen to the tire noise; an acoustic sensor is used to obtain information on road condition by registering the acoustic waves emitted by the tires in [9]. The treads of tires can be supplied with sensors for measuring stress and strain. In [10], sensors of tire-tread deformation are applied to obtain information on the tire-road condition. The use of optical and acoustic sensors is particularly promising for detecting wet surfaces and the risk of aquaplaning. However, the solution process is technically very complicated and expensive. Despite several experiments has verified the effectiveness and accuracy, all these cause-based methods require special sensors and are of high cost. Effect-based approaches try to quantify the friction impacts between the tire and the road. The friction impacts show on the tire in the forms of tire-tread deformation and wheel slipping. In [11], an online algorithm based on the friction curve is presented and the performance of the algorithm is evaluated in both simulation and experiments. However, when the vehicle model becomes complicated, the demand for computing power could be high due to computational complexity. To obtain a better control performance on the slip ratio, an intelligent tire system is proposed in [12], and the various tire friction information is estimated based on acceleration signals. In [13], a slip-slope method is presented based on a recursive least-squares algorithm. However, to achieve an accurate estimation performance, the proposed method relies on large tire slip greatly. If the tire slip is extremely small, the system will not be able to identify the friction coefficient information. In [14], a dynamics-based estimation method of the TRFC is presented and simulation results show that the reliability of the anti-lock brake system has been enhanced. In [15], a parameter identification method based on differences among tire forces generated by in-wheel motors is proposed to estimate the cornering stiffness coefficient and the TRFC. In order to realize the vehicle velocity control with unknown road friction conditions, an adaptive function is presented in the controller design based on the approximate estimation of the TRFC in [16]. In [17], three estimation algorithms are presented based on the calculation of slip-slope. However, all these methods are effective only when the vehicle velocity can be measured from sensor systems.

Nonetheless, in practice, vehicle velocities are not measurable but are usually estimated. For the velocity estimation, many different approaches have been proposed. A kinematics-based algorithm is presented in [18], which can estimate the lateral velocity and the TRFC simultaneously. In [19], a sliding mode observer is proposed to estimate vehicle acceleration, which can be further used for the estimation of velocity. In [20], a modular observer is presented for the estimation of vehicle velocity. In this method, the Dugoff's tire friction model is applied and the longitudinal tire forces are used as inputs to the velocity observer. Errors including measurement noises from sensors are considered in the design of velocity estimation approach for a mobile robot proposed in [21]. In [22], a fixed gain structure observer is proposed for the estimation of vehicle velocities based on the acceleration measurements. A couple of observers are proposed in [23] for the estimation of longitudinal velocity and lateral velocity, respectively. However, only when the tire works in the linear region condition is considered in the proposed method which may bring great limitations in real driving process. In addition to the observer methods mentioned above, the extended Kalman filter-based approaches are utilized in the literature [24,25] as well. Besides, in order to deal with the effect of the parameter uncertainties, a nonlinear observer based on the differential inclusion theory is proposed to estimate the uncertainties within a finite time [26,27]. However, the TRFC is regarded as a known state information in most of these estimation methods. To the best our knowledge, few published papers have considered the problem of estimating the vehicle velocity and the TRFC simultaneously.

In this paper, a nonlinear modular observer is developed to estimate the longitudinal and lateral velocities together with the TRFC. First, the longitudinal tire forces are estimated based on a filter observer. Then inspired by [28], a vehicle velocity and TRFC estimation observer is proposed based on the calculation of lateral tire forces. The convergence of the observer is analyzed based on the Lyapunov method, and simulation results are presented for performance evaluation. In comparison with existing works, the estimation of the TRFC depending on vehicle lateral tire friction model is incorporated into the observer design, so that the road surface information can be considered into the estimation of vehicle velocity to ensure the estimation results more accurate and reliable.

The rest of this paper is organized as follows. The vehicle dynamics and tire friction models are discussed

in Sect. 2. The proposed observer is detailed in Sect. 3, and the convergence analysis is presented in Sect. 4. Simulation tests in different driving conditions performed in CarSim are presented in Sect. 5. Conclusions are presented in Sect. 6.

2 Model development

Environmental factors such as road surface affect vehicle dynamics and thus vehicle motions greatly. In this section, to analyze the effect of road surface on vehicle dynamics, a vehicle dynamical model is introduced to describe the longitudinal and lateral motions first. Then, the tire friction model and wheel dynamics model are presented. These models will be utilized as a foundation for the design of the modular observer in Sect. 3.

2.1 Vehicle model

Assume that the vehicle is moving on a flat road without road grade or bank angle, the vehicle dynamics can be expressed as follows [29]:

$$\begin{aligned} \dot{v}_x &= r v_y + a_x \\ \dot{v}_y &= -r v_x + a_y \end{aligned} \tag{1}$$

where r is the yaw rate, v_x and v_y are the longitudinal and lateral velocities of the vehicle, respectively. The longitudinal and lateral acceleration rates a_x and a_y in (1) can be further expressed as follows :

$$\begin{aligned} a_x &= \frac{1}{m}\sum_{i=1}^{4}(F_{\mathrm{xi}}\cos\delta_i - F_{\mathrm{yi}}\sin\delta_i) \\ a_y &= \frac{1}{m}\sum_{i=1}^{4}(F_{\mathrm{xi}}\sin\delta_i + F_{\mathrm{yi}}\cos\delta_i) \end{aligned} \tag{2}$$

where F_{xi} and F_{yi} are the longitudinal and lateral forces of the ith wheel, respectively; δ_i denotes the steering angle of the corresponding wheel and m is the vehicle mass.

Remark 1 The surface roughness is usually represented by the friction coefficient of the road and the structural depth of the road surface. This study focuses on the estimation of the tire-road friction coefficient, and the structural depth of the road surface is not considered. Therefore, as proposed in literature [20,30], and [31], it is assumed that the road grade and the bank angle are both equal to zero. Otherwise, more complicated vehicle dynamics should be used considering road profile estimations which is not the focus of this study. Besides, the road grade angle and road bank angle don't affect the validity of the proposed algorithm theoretically but only have an effect on the complexity of the vehicle dynamics model when they are able to be known exactly. Specifically, the road grade angle influences nominal forces and longitudinal acceleration by producing components of the vehicle gravity, and the bank angle mainly has an influence on the lateral acceleration. For simplicity and also as a kind of actual road situations, the road grade and the bank angle are not taken into consideration.

2.2 Tire friction model

The model of the tire-road contact force is complicated because it is affected by a wide variety of parameters including the tire characters such as tire cornering stiffness, tire distortion and slip, radial deflection, tire-road friction coefficient and nominal tire load acting on each tire [32]. In this paper, the tire force is assumed to be at the center of the contact patch, the following expression is used to represent the lateral force on each tire [33]:

$$F_{\mathrm{yi}} = \begin{cases} \mu F_{\mathrm{zi}} g(\alpha_i), & \text{if } |q(\alpha_i)| \le 3 \\ \mu F_{\mathrm{zi}}, & \text{if } |q(\alpha_i)| > 3 \end{cases} \tag{3}$$

where

$$\begin{aligned} g(\alpha_i) &= \left\{ |q(\alpha_i)| - \frac{|q(\alpha_i)|^2}{3} + \frac{|q(\alpha_i)|^3}{27} \right\} \mathrm{sign}(\alpha_i) \\ q(\alpha_i) &= \frac{C_y \tan\alpha_i}{\mu F_{\mathrm{zi}}} \end{aligned} \tag{4}$$

in which μ is the TRFC and C_y denotes the cornering stiffness. The slip angle of the ith tire α_i in (3) is defined as the angle between the orientation of the tire and the orientation of the velocity vector of the ith wheel as shown in Fig. 2, which can be calculated as follows:

$$\alpha_i = \delta_i - \theta_i \tag{5}$$

where θ_i is the angle that the velocity vector of the ith wheel makes with the longitudinal axis of the vehicle; δ_i denotes the steering angle of the corresponding wheel. Therefore, the slip angles are similarly given by:

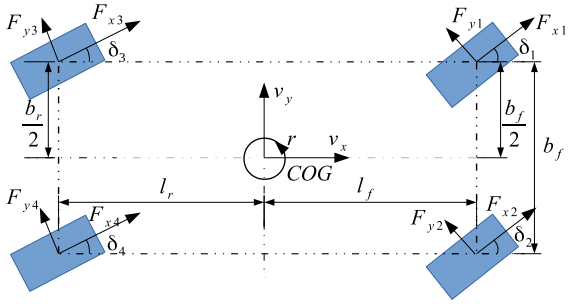

Fig. 1 Vehicle model

$$\begin{aligned}
\alpha_1 &= \delta_1 - \arctan\left(\frac{v_y + l_f \cdot r}{v_x - \frac{b_f}{2} \cdot r}\right)\\
\alpha_2 &= \delta_2 - \arctan\left(\frac{v_y + l_f \cdot r}{v_x + \frac{b_f}{2} \cdot r}\right)\\
\alpha_3 &= \delta_3 - \arctan\left(\frac{v_y - l_r \cdot r}{v_x - \frac{b_r}{2} \cdot r}\right)\\
\alpha_4 &= \delta_4 - \arctan\left(\frac{v_y - l_r \cdot r}{v_x + \frac{b_r}{2} \cdot r}\right)
\end{aligned} \tag{6}$$

where l_f, l_r, b_f and b_r are lengths illustrated in Fig. 1. Taking moments about the contact point of the rear and front tires, respectively:

$$\begin{aligned}
(F_{z1} + F_{z2})(l_f + l_r) + \mathrm{ma}_x h - \mathrm{mgl}_r &= 0\\
(F_{z3} + F_{z4})(l_f + l_r) - \mathrm{ma}_x h - \mathrm{mgl}_f &= 0
\end{aligned} \tag{7}$$

where g represents the gravitational acceleration and h is the height of the vehicle's center of gravity. The load transfers of the front and rear wheels $\triangle F_{\mathrm{zf}}, \triangle F_{\mathrm{zr}}$ from the inner to the outer wheels in the steady-state cornering motion with centripetal acceleration a_y follows from the formula [33]:

$$\begin{aligned}
\triangle F_{\mathrm{zf}} &= \frac{\mathrm{mha}_y(l_r \cdot g - \mathrm{ha}_x)}{(l_f + l_r)g \cdot b_f}\\
\triangle F_{\mathrm{zr}} &= \frac{\mathrm{mha}_y(l_f \cdot g + \mathrm{ha}_x)}{(l_f + l_r)g \cdot b_r}.
\end{aligned} \tag{8}$$

The resulting vertical loads become, after considering the left and right increments in load:

$$\begin{aligned}
F_{z1} &= \frac{1}{2}(F_{z1} + F_{z2}) - \triangle F_{\mathrm{zf}}\\
F_{z2} &= \frac{1}{2}(F_{z1} + F_{z2}) + \triangle F_{\mathrm{zf}}
\end{aligned}$$

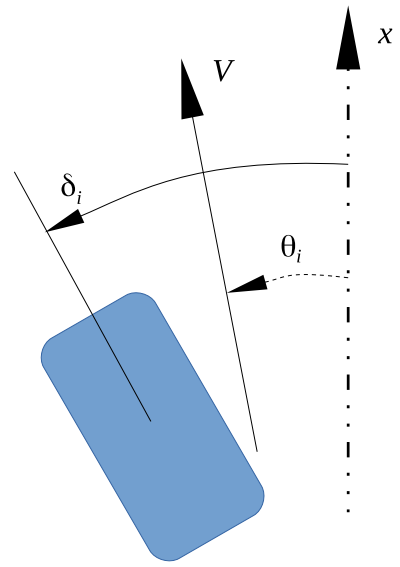

Fig. 2 Tire slip angle

$$\begin{aligned}
F_{z3} &= \frac{1}{2}(F_{z3} + F_{z4}) - \triangle F_{\mathrm{zr}}\\
F_{z4} &= \frac{1}{2}(F_{z3} + F_{z4}) + \triangle F_{\mathrm{zr}}.
\end{aligned} \tag{9}$$

Therefore, based on (7)–(9), the normal forces acting on the ith wheel can be calculated as:

$$\begin{aligned}
F_{z1} &= \frac{m(l_r \cdot g - \mathrm{ha}_x)}{2(l_f + l_r)} - \frac{\mathrm{mha}_y(l_r \cdot g - \mathrm{ha}_x)}{(l_f + l_r)g \cdot b_f}\\
F_{z2} &= \frac{m(l_r \cdot g - \mathrm{ha}_x)}{2(l_f + l_r)} + \frac{\mathrm{mha}_y(l_r \cdot g - \mathrm{ha}_x)}{(l_f + l_r)g \cdot b_f}\\
F_{z3} &= \frac{m(l_f \cdot g + \mathrm{ha}_x)}{2(l_f + l_r)} - \frac{\mathrm{mha}_y(l_f \cdot g + \mathrm{ha}_x)}{(l_f + l_r)g \cdot b_r}\\
F_{z4} &= \frac{m(l_f \cdot g + \mathrm{ha}_x)}{2(l_f + l_r)} + \frac{\mathrm{mha}_y(l_f \cdot g + \mathrm{ha}_x)}{(l_f + l_r)g \cdot b_r}
\end{aligned} \tag{10}$$

where g represents the gravitational acceleration and h is the height of the vehicle's center of gravity.

2.3 Wheel dynamics

As shown in Fig. 3, by assuming that the rolling resistance and the tire deformation are negligible, the wheel dynamics equation can be expressed as below [34]:

$$I_\omega \dot{\omega}_i = T_{\mathrm{di}} + T_{\mathrm{bi}} - R_{\mathrm{eff}} F_{\mathrm{xi}} - B\omega_i \quad i = 1, 2, 3, 4 \tag{11}$$

where I_ω is the inertia of the wheel; B is the equivalent bearing and friction coefficient; T_{di} and T_{bi} refer to

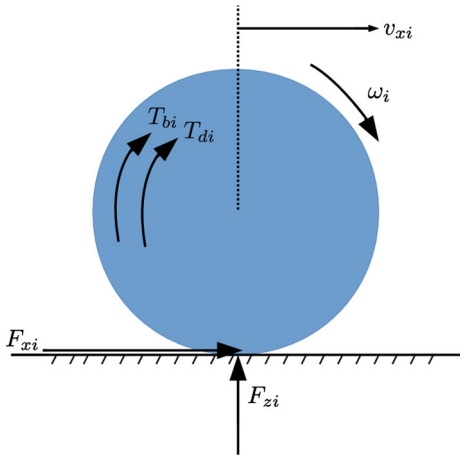

Fig. 3 Wheel dynamics model

the drive torque and brake torque on the ith wheel, respectively; R_{eff} represents the effective radius of tire and ω_i is the wheel angular velocity of the ith wheel.

3 Observer design

In this section, a nonlinear modular observer is designed for the estimation of vehicle states. The observer structure is illustrated in Fig. 4, in which the yaw rate, steering wheel angles, longitudinal acceleration and lateral acceleration can be measured from low cost sensors.

The longitudinal tire force of each tire is first estimated based on a filter observer, which is denoted as $\hat{F}_{\text{xi}}$. Then, according to the vehicle model presented in (2), $h_y \triangleq \sum_{i=1}^{4} F_{\text{yi}}^{\text{cal}} \cos\delta_i$ can be calculated. Besides, the estimated value of the lateral force can be obtained from the lateral tire model presented in (3), which is denoted as $\hat{F}_{\text{yi}}$. The design of the observer is detailed in the following subsections.

3.1 Estimation of longitudinal tire forces

Suppose that the wheel torque is available, $\dot{\omega}_i$ can be calculated based on the wheel dynamics equation described in (11):

$$\dot{\omega}_i = -\frac{B}{I_\omega}\omega_i + T(u,t) + f(w_i,t) \tag{12}$$

where $f(w_i,t) \triangleq -\frac{R_{\text{eff}}}{I_\omega}F_{\text{xi}}$ and $T(u,t) \triangleq \frac{T_{\text{di}}+T_{\text{bi}}}{I_\omega}$. Then, a filter observer for the wheel angular velocity is designed as follows:

$$\dot{\hat{\omega}}_i = -\frac{B}{I_\omega}\hat{\omega}_i + T(u,t) + \tau_i(t) \tag{13}$$

in which

$$\begin{aligned}\tau_i(t) &= \phi_1(e_i) + \int_0^t \phi_2(e_i)\mathrm{d}t - \frac{B}{I_\omega}e_i\\ \phi_1(e_i) &= k_{i1}|e_i|^{\frac{1}{2}}\text{sign}(e_i) + k_{i2}e_i\\ \phi_2(e_i) &= k_{i3}\text{sign}(e_i) + k_{i4}e_i.\end{aligned} \tag{14}$$

The estimate error of the wheel angular velocity e_i is defined as $e_i \triangleq \omega_i - \hat{\omega}_i$, then

$$\begin{aligned}\dot{e}_i &= \dot{\omega}_i - \dot{\hat{\omega}}_i = -\frac{B}{I_\omega}e_i + f(w_i,t) - \tau_i(t)\\ &= f(w_i,t) - \phi_1(e_i) - \int_0^t \phi_2(e_i)\mathrm{d}t.\end{aligned} \tag{15}$$

Because $-\frac{R_{\text{eff}}}{I_\omega}\dot{F}_{\text{xi}}$ is bounded in real driving conditions, denote

$$\begin{aligned}\dot{e}_i &= e_{i1} - \phi_1(e_i)\\ \dot{e}_{i1} &= -\phi_2(e_i) + \dot{\rho}_i\end{aligned} \tag{16}$$

where

$$\begin{aligned}e_{i1} &= f(w_i,t) - \int_0^t \phi_2(e_i)\mathrm{d}t\\ \rho_i &= f(w_i,t)\end{aligned} \tag{17}$$

then the derivative of e_i and e_{i1} can be calculated as follows:

$$\begin{aligned}\dot{e}_i &= -k_{i1}|e_i|^{\frac{1}{2}}\text{sign}(e_i) - k_{i2}e_i + e_{i1}\\ \dot{e}_{i1} &= -k_{i3}\text{sign}(e_i) - k_{i4}e_i + \dot{\rho}_i.\end{aligned} \tag{18}$$

Theorem 1 *Suppose that the derivative of ρ is globally bounded by $|\dot{\rho}_i| \le b_{i1} + b_{i2}|e_i|$ for some constants $b_{i1}, b_{i2} > 0$, then the gains k_i can be selected such that $k_{i1} > 2\sqrt{b_{i1}}$, $k_{i2} > \sqrt{b_{i2}}$, $k_{i3} > 0$, $k_{i4} > 0$ so that the system is finite-time stable. Furthermore, the term $\int_0^t \phi_2(e_i)\mathrm{d}t$ provides a smooth estimation of ρ_i in finite time.*

Proof The Lyapunov function $V(e_i) \in \mathcal{R}$ is first designed as follows:

$$\begin{aligned}V(e_i) = \frac{1}{2}\Big[k_{i1}|e_i|^{\frac{1}{2}}\text{sign}(e_i) + k_{i2}e_i - e_{i1}\Big]^2\\ + 2k_{i3}|e_i| + k_{i4}e_i^2 + \frac{1}{2}e_{i1}^2.\end{aligned} \tag{19}$$

Let $\varrho_i = [|e_i|^{\frac{1}{2}}\text{sign}(e_i) \quad e_i \quad e_{i1}]^T$, then $V(e_i)$ can be written as $V(e_i) = {\varrho_i}^T H_i \varrho_i$, where

$$H_i = \frac{1}{2}\begin{bmatrix} (4k_{i3} + k_{i1}^2) & k_{i1}k_{i2} & -k_{i1} \\ k_{i1}k_{i2} & (2k_{i4} + k_{i2}^2) & -k_{i2} \\ -k_{i1} & -k_{i2} & 2 \end{bmatrix} \tag{20}$$

and satisfies $\lambda_{\min}\{H_i\}\| \varrho_i \|^2 \leq V(e_i) \leq \lambda_{max}\{H_i\}\| \varrho_i \|^2$, in which $\| \varrho_i \|^2 = |e_i| + e_i^2 + e_{i1}^2$.

After taking derivatives of (19), the following results can be obtained:

$$\begin{aligned} \dot{V}(e_i) = &-\frac{1}{\sqrt{|e_i|}}{\varrho_i}^T A_{i1}\varrho_i - {\varrho_i}^T A_{i2}\varrho_i \\ &+ \dot{\rho}_i(-k_{i1}\varrho_{i1} - k_{i2}\varrho_{i2} + 2\varrho_{i3}) \end{aligned} \tag{21}$$

in which

$$\begin{aligned} A_{i1} &= \frac{k_{i1}}{2}\begin{bmatrix} (2k_{i3} + k_{i1}^2) & 0 & -k_{i1} \\ 0 & (2k_{i4} + 5k_{i2}^2) & -3k_{i2} \\ -k_{i1} & -3k_{i2} & 1 \end{bmatrix} \\ A_{i2} &= k_{i2}\begin{bmatrix} k_{i3} + 2k_{i1}^2 & 0 & 0 \\ 0 & (k_{i4} + k_{i2}^2) & -k_{i2} \\ 0 & -k_{i2} & 1 \end{bmatrix} \end{aligned} \tag{22}$$

where $\dot{\rho}_i$ is upper-bounded by $|\dot{\rho}_i| \leq b_{i1} + b_{i2}|e_i|$, then

$$\dot{\rho}_i(-k_{i1}\varrho_{i1} - k_{i2}\varrho_{i2} + 2\varrho_{i3}) \leq G_{i1} + G_{i2} = G_i \tag{23}$$

where

$$\begin{aligned} G_{i1} &= (b_{i1} + b_{i2}|e_i|)(k_{i1}|e_i|^{\frac{1}{2}} + k_{i2}|e_i|) \\ &= \left(\frac{k_{i1}}{|e_i|^{\frac{1}{2}}} + k_{i2}\right)(b_{i1}\varrho_{i1}^2 + b_{i2}\varrho_{i2}^2) \\ G_{i2} &= 2e_{i1}(b_{i1} + b_{i2}|e_i|) \end{aligned} \tag{24}$$

then G_i can be expressed as:

$$G_i = \begin{cases} \frac{1}{|e_i|^{\frac{1}{2}}}{\varrho_i}^T B_{i1}\varrho_i + {\varrho_i}^T B_{i2}\varrho_i, & \text{if } e_i \geq 0 \\ \frac{1}{|e_i|^{\frac{1}{2}}}{\varrho_i}^T B_{i1}^{'}\varrho_i + {\varrho_i}^T B_{i2}^{'}\varrho_i, & \text{if } e_i < 0 \end{cases} \tag{25}$$

in which

$$\begin{aligned} B_{i1} &= k_{i1}\begin{bmatrix} b_{i1} & 0 & \frac{b_{i1}}{k_{i1}} \\ 0 & b_{i2} & 0 \\ \frac{b_{i1}}{k_{i1}} & 0 & 0 \end{bmatrix}, \\ B_{i1}^{'} &= k_{i1}\begin{bmatrix} b_{i1} & 0 & -\frac{b_{i1}}{k_{i1}} \\ 0 & b_{i2} & 0 \\ -\frac{b_{i1}}{k_{i1}} & 0 & 0 \end{bmatrix} \\ B_{i2} &= k_{i2}\begin{bmatrix} b_{i1} & 0 & 0 \\ 0 & b_{i2} & \frac{b_{i2}}{k_{i2}} \\ 0 & \frac{b_{i2}}{k_{i2}} & 0 \end{bmatrix}, \\ B_{i2}^{'} &= k_{i2}\begin{bmatrix} b_{i1} & 0 & 0 \\ 0 & b_{i2} & -\frac{b_{i2}}{k_{i2}} \\ 0 & -\frac{b_{i2}}{k_{i2}} & 0 \end{bmatrix} \end{aligned} \tag{26}$$

Hence, $\dot{V}(e_i) \leq$

$$\begin{cases} -\frac{1}{|e_i|^{\frac{1}{2}}}{\varrho_i}^T(A_{i1} - B_{i1})\varrho_i - {\varrho_i}^T(A_{i2} - B_{i2})\varrho_i, & e_i \geq 0 \\ -\frac{1}{|e_i|^{\frac{1}{2}}}{\varrho_i}^T(A_{i1} - B_{i1}^{'})\varrho_i - {\varrho_i}^T(A_{i2} - B_{i2}^{'})\varrho_i, & e_i < 0. \end{cases} \tag{27}$$

It can be demonstrated that the terms $(A_{i1} - B_{i1})$, $(A_{i2} - B_{i2})$, $(A_{i1} - B_{i1}^{'})$ and $(A_{i2} - B_{i2}^{'})$ are all positive definite, $\dot{V}(e_i) \leq 0$. So the observer system with the robust term $\tau_i(t)$ ensures the error dynamics converges to zero in finite time. □

Theorem 1 ensures that as $t \to \infty$, $e_{i1} \to 0$. Therefore, the estimated longitudinal tire force can be obtained as:

$$\hat{F}_{\text{xi}} = -\frac{I_w}{R_{\text{eff}}}\hat{\rho}_i = -\frac{I_w}{R_{\text{eff}}}\int_0^t \phi_2(e_i). \tag{28}$$

Then based on (2), h_y can be calculated as follows:

$$h_y = ma_y - \sum_{i=1}^{4}\hat{F}_{\text{xi}}\sin\delta_i. \tag{29}$$

3.2 Observer design for vehicle velocity and TRFC

Observer for longitudinal and lateral velocities together with the tire-road friction coefficient is designed in this subsection, which is based on the calculation of the lateral tire force.

Assumption 1 The value of the tire-road friction coefficient is constant for the same road segment: $\dot{\mu} = 0$.

The vehicle states and the estimation of vehicle states are defined as $x = [v_x \quad v_y \quad \mu]^T$ and $\hat{x} = [\hat{v}_x \quad \hat{v}_y \quad \hat{\mu}]^T$, respectively. The observer for vehicle velocity and the tire-road friction coefficient is designed as follows:

$$\begin{aligned}
\dot{\hat{x}}_1 &= r\hat{x}_2 + a_x + l_1\left(\frac{1}{4}\sum_{i=1}^{4} v_{iw} - \hat{x}_1\right)\\
\dot{\hat{x}}_2 &= -r\hat{x}_1 + a_y - l_2\left(h_y - \sum_{i=1}^{4}\hat{F}_{\mathrm{yi}}\cos\delta_i\right)\\
\dot{\hat{x}}_3 &= l_3\left(h_y - \sum_{i=1}^{4}\hat{F}_{\mathrm{yi}}\cos\delta_i\right)
\end{aligned} \tag{30}$$

where l_1, l_2 and l_3 are observer gains and v_{iw} is the longitudinal velocity of the ith wheel which can be calculated as

$$v_{iw} = \begin{cases} \omega_i R_{\mathrm{eff}}\cos\delta_i + \omega_i r, & \text{if } i = 1, 2\\ \omega_i R_{\mathrm{eff}}\cos\delta_i - \omega_i r, & \text{if } i = 3, 4. \end{cases} \tag{31}$$

In (30), the estimated tire force $\hat{F}_{\mathrm{yi}}$ is obtained by substituting the estimated vehicle states $\hat{x}$ in the tire friction model proposed in (3). The estimate error $\tilde{x}(t) \triangleq x(t) - \hat{x}(t)$ can be expressed as follows:

$$\begin{aligned}
\dot{\tilde{x}}_1 &= r\tilde{x}_2 - l_1\tilde{x}_1 + u_1\\
\dot{\tilde{x}}_2 &= -r\tilde{x}_1 + l_2\sum_{i=1}^{4}(F_{\mathrm{yi}} - \hat{F}_{\mathrm{yi}})\cos\delta_i + u_2\\
\dot{\tilde{x}}_3 &= -l_3\sum_{i=1}^{4}(F_{\mathrm{yi}} - \hat{F}_{\mathrm{yi}})\cos\delta_i + u_3
\end{aligned} \tag{32}$$

where, $u_1(t), u_2(t), u_3(t) \in \mathcal{R}$ are the signals defined as follows:

$$\begin{aligned}
u_1 &\triangleq \frac{l_1}{4}\sum_{i=1}^{4}(v_x - v_{iw})\\
u_2 &\triangleq l_2\left(h_y - \sum_{i=1}^{4}F_{\mathrm{yi}}\cos\delta_i\right)\\
u_3 &\triangleq -l_3\left(h_y - \sum_{i=1}^{4}F_{\mathrm{yi}}\cos\delta_i\right)
\end{aligned} \tag{33}$$

where u_{obs} is defined as $u_{\mathrm{obs}} \triangleq [u_1 \quad u_2 \quad u_3]^T \in \mathcal{D}_{uobs}$ and $\mathcal{D}_{uobs}$ refers to the domain of the signals.

Remark 2 The equation $v_{iw} = \omega_i R_{\mathrm{eff}}\cos\delta_i$ is used to estimate the vehicle longitudinal velocity to simplify the relationship detailed in (27) and h_y is calculated from (25). Besides, as to be seen in the stability analysis detailed in Sect. 4 and the simulation tests shown in Sect. 5, the effect of the signals u_{obs} to the observer system can be ignored.

4 Observer convergence analysis

In the following analysis, it is proved that the designed observer is input-to-state stable (ISS) despite of the existence of external inputs. To analyze the stability property of the modular observer, the following two Lemmas are firstly proposed.

Lemma 1 $\frac{\partial F_{\mathrm{yi}}}{\partial v_y} \le 0$ *can be obtained when* $v_x > max\{|\frac{b_f}{2}\cdot r|, |\frac{b_r}{2}\cdot r|\}$.

Proof According to (3), F_{yi} can be described by the following ones:

$$F_{\mathrm{yi}} = \mu F_{\mathrm{zi}}\cdot h(\alpha_i) \tag{34}$$

in which $h(\alpha_i)$ can be expressed below:

$$h(\alpha_i) \triangleq \begin{cases} g(\alpha_i), & \text{if } |q(\alpha_i)| \le 3\\ 1, & \text{if } |q(\alpha_i)| > 3. \end{cases} \tag{35}$$

The derivatives of F_{yi} with respect to v_y can be calculated as:

$$\frac{\partial F_{\mathrm{yi}}}{\partial v_y} = \mu F_{\mathrm{zi}}\cdot\frac{\partial h(\alpha_i)}{\partial \alpha_i}\cdot\frac{\partial \alpha_i}{\partial v_y}. \tag{36}$$

If $|q(\alpha_i)| > 3$, $h(\alpha_i) = 1$, then

$$\frac{\partial h(\alpha_i)}{\partial \alpha_i} = 0. \tag{37}$$

Otherwise, if $|q(\alpha_i)| \le 3$, then

$$\frac{\partial h(\alpha_i)}{\partial \alpha_i} = \frac{C_y}{\mu F_{\mathrm{zi}}}\left(\frac{C_y}{3\mu F_{\mathrm{zi}}}|\tan\alpha_i| - 1\right)^2\cdot\sec^2\alpha_i \ge 0. \tag{38}$$

According to (37) and (38), $\frac{\partial h(\alpha_i)}{\partial \alpha_i} \ge 0$ can be obtained. Based on (5), after taking the derivative of the side slip angle α_i with respect to v_y, it's easy to demonstrate that $\frac{\partial \alpha_i}{\partial v_y} < 0$ when $v_x > \max\{|\frac{b_f}{2}\cdot r|, |\frac{b_r}{2}\cdot r|\}$ is satisfied.

Therefore according to the analysis above, it can be concluded that $\frac{\partial F_{\mathrm{yi}}}{\partial v_y} \le 0$ on the condition that $v_x > \max\{|\frac{b_f}{2}\cdot r|, |\frac{b_r}{2}\cdot r|\}$. □

Lemma 2 *There exist positive constants c_1, c_2, c_3 that the following relationships can always be true for $x(t)$, $\hat{x}(t) \subseteq \mathcal{R}_3$:*

$$\begin{aligned}
&\tilde{x}_3 \sum_{i=1}^{4}(F_{\mathrm{yi}} - \hat{F}_{\mathrm{yi}})\cos\delta_i \\
&\quad \le c_1|\tilde{x}_1||\tilde{x}_3| + c_2|\tilde{x}_2||\tilde{x}_3| + c_3\tilde{x}_3^2 \\
&\tilde{x}_2 \sum_{i=1}^{4}(F_{\mathrm{yi}} - \hat{F}_{\mathrm{yi}})\cos\delta_i \\
&\quad \le c_1|\tilde{x}_1||\tilde{x}_2| - c_2\tilde{x}_2^2 + c_3|\tilde{x}_2||\tilde{x}_3|.
\end{aligned} \tag{39}$$

Proof By using Lagrange mean value theorem, the following results can be obtained:

$$\begin{aligned}
\sum_{i=1}^{4}(F_{\mathrm{yi}} - \hat{F}_{\mathrm{yi}})\cos\delta_i = &\sum_{i=1}^{4}\frac{\partial F_{\mathrm{yi}}}{\partial x_1}(\overline{x}_i)\cos\delta_i\tilde{x}_1 \\
&+ \sum_{i=1}^{4}\frac{\partial F_{\mathrm{yi}}}{\partial x_2}(\overline{x}_i)\cos\delta_i\tilde{x}_2 \\
&+ \sum_{i=1}^{4}\frac{\partial F_{\mathrm{yi}}}{\partial x_3}(\overline{x}_i)\cos\delta_i\tilde{x}_3
\end{aligned} \tag{40}$$

where $\overline{x} = [\overline{x}_1 \quad \overline{x}_2 \quad \overline{x}_3]^T$ is a point between x_i and $\hat{x}_i$. After multiplying (40) with $\tilde{x}_3$, the following equation can be obtained:

$$\begin{aligned}
&\tilde{x}_3 \sum_{i=1}^{4}(F_{\mathrm{yi}} - \hat{F}_{\mathrm{yi}})\cos\delta_i \\
&= \sum_{i=1}^{4}\frac{\partial F_{\mathrm{yi}}}{\partial x_1}(\overline{x}_i)\cos\delta_i\tilde{x}_1\tilde{x}_3 \\
&\quad + \sum_{i=1}^{4}\frac{\partial F_{\mathrm{yi}}}{\partial x_2}(\overline{x}_i)\cos\delta_i\tilde{x}_2\tilde{x}_3 \\
&\quad + \sum_{i=1}^{4}\frac{\partial F_{\mathrm{yi}}}{\partial x_3}(\overline{x}_i)\cos\delta_i\tilde{x}_3^2.
\end{aligned} \tag{41}$$

According to Lemma 1, $\frac{\partial F_{\mathrm{yi}}}{\partial v_y} \le 0$ when certain conditions are satisfied. Therefore the upper bounds of $\frac{\partial F_{\mathrm{yi}}}{\partial x_1}$, $\frac{\partial F_{\mathrm{yi}}}{\partial x_2}$, $\frac{\partial F_{\mathrm{yi}}}{\partial x_3}$ can be found and assuming that c_1, $-c_2$, and c_3 are upper bounds of $\sum_{i=1}^{4}\frac{\partial F_{\mathrm{yi}}}{\partial x_1}\cos\delta_i$, $\sum_{i=1}^{4}\frac{\partial F_{\mathrm{yi}}}{\partial x_2}\cos\delta_i$, and $\sum_{i=1}^{4}\frac{\partial F_{\mathrm{yi}}}{\partial x_3}\cos\delta_i$, respectively, which can be expressed in the following way:

Table 1 Vehicle parameters

Parameters (units)	Value
m (kg)	1723
C_y (N · rad^{-1})	19350
l_f (m)	1.232
l_r (m)	1.468
R_{eff} (m)	0.353
b_f (m)	1
b_r (m)	1
I_ω (kg · m^2)	1.5
h (m)	0.46

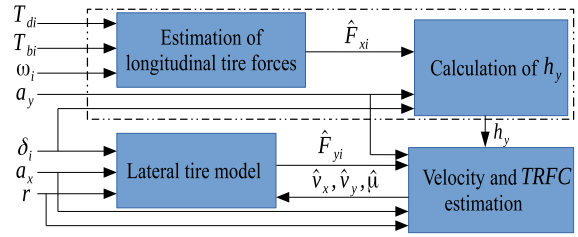

Fig. 4 Observer structure

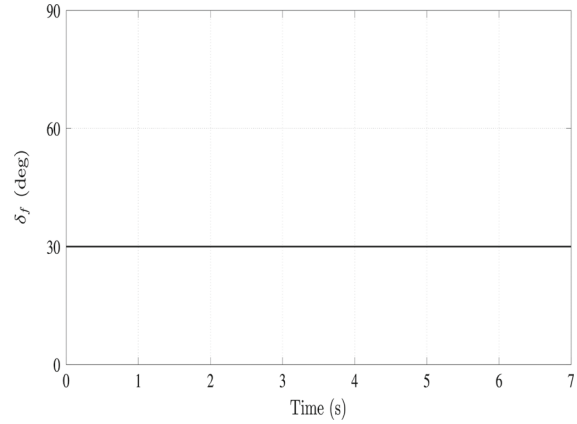

Fig. 5 Front wheel steering angle on a high-μ case

$$\begin{aligned}
&\sum_{i=1}^{4}\frac{\partial F_{\mathrm{yi}}}{\partial x_1}(\overline{x}_i)\cos\delta_i \le c_1 \\
&\sum_{i=1}^{4}\frac{\partial F_{\mathrm{yi}}}{\partial x_2}(\overline{x}_i)\cos\delta_i \le -c_2 \\
&\sum_{i=1}^{4}\frac{\partial F_{\mathrm{yi}}}{\partial x_3}(\overline{x}_i)\cos\delta_i \le c_3.
\end{aligned} \tag{42}$$

Fig. 6 Longitudinal tire forces estimation on a high-μ case

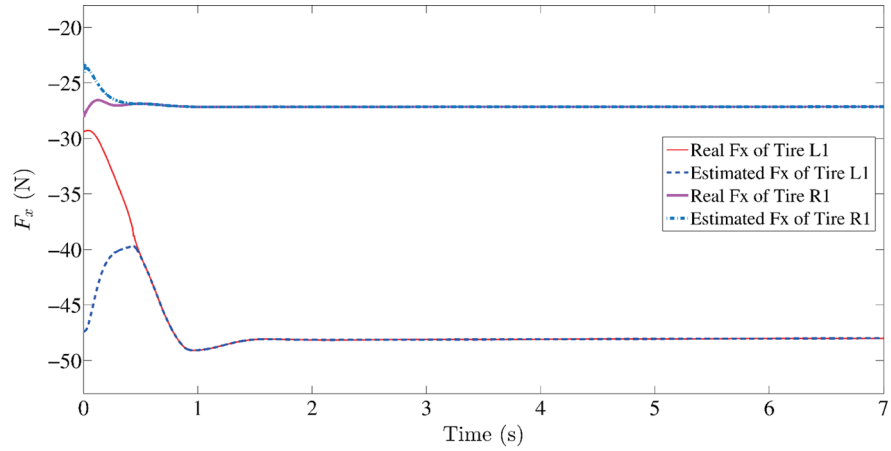

(a) Estimated errors of the front tire longitudinal forces

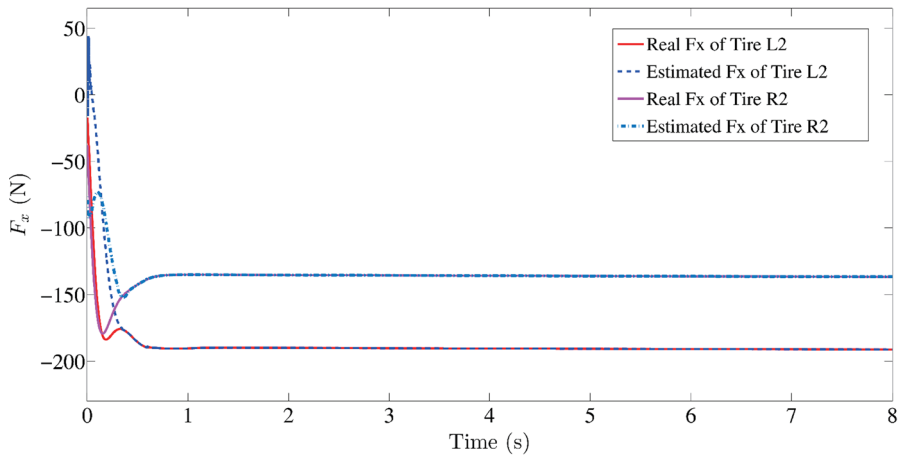

(b) Estimated errors of the rear tire longitudinal forces

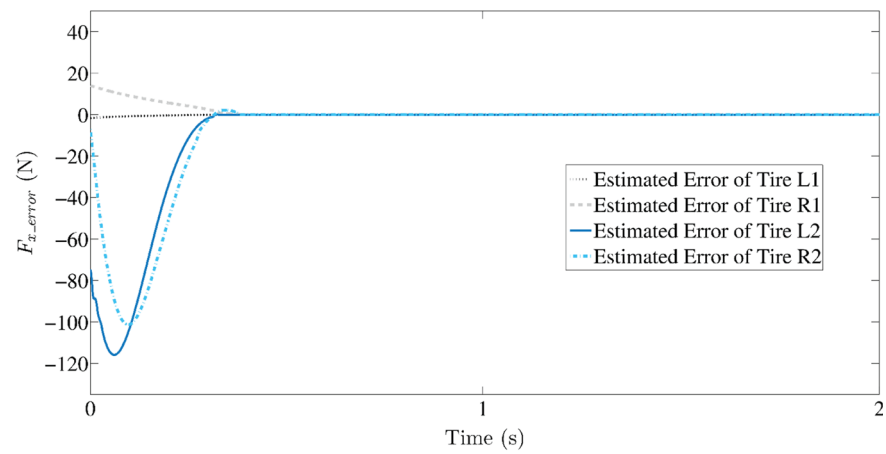

(c) Estimated errors of the longitudinal forces

Fig. 7 States estimation on a high-μ case with a small steering wheel angle

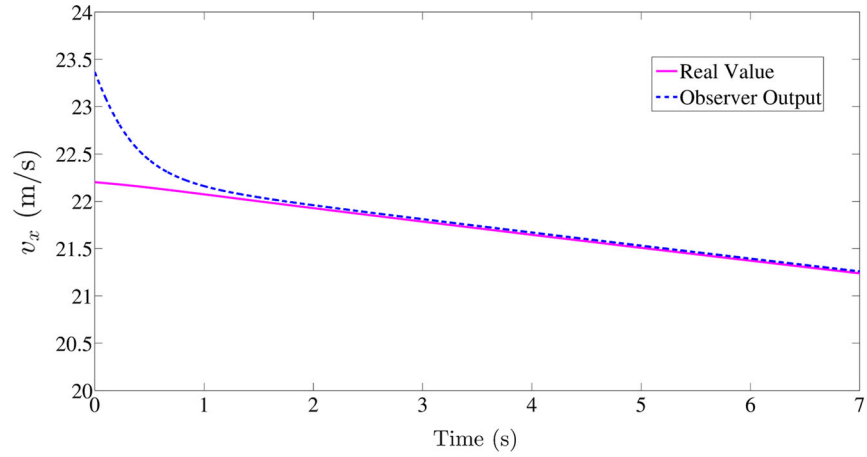

(a) Longitudinal velocity estimation

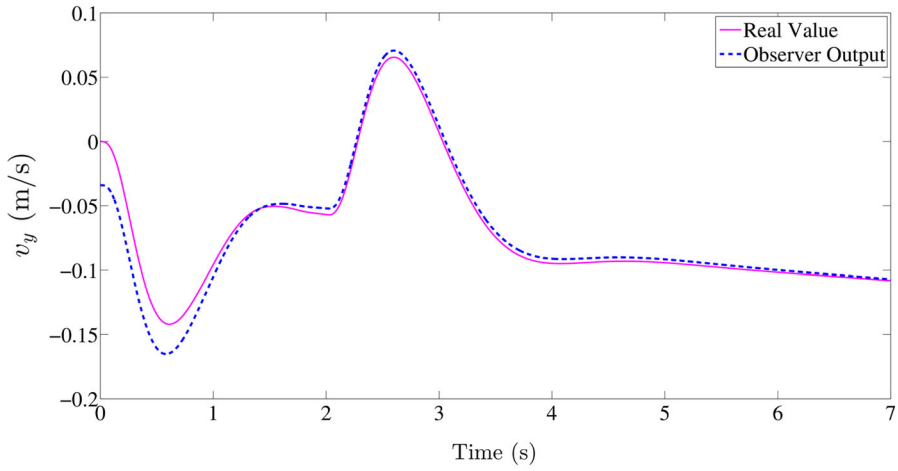

(b) Lateral velocity estimation

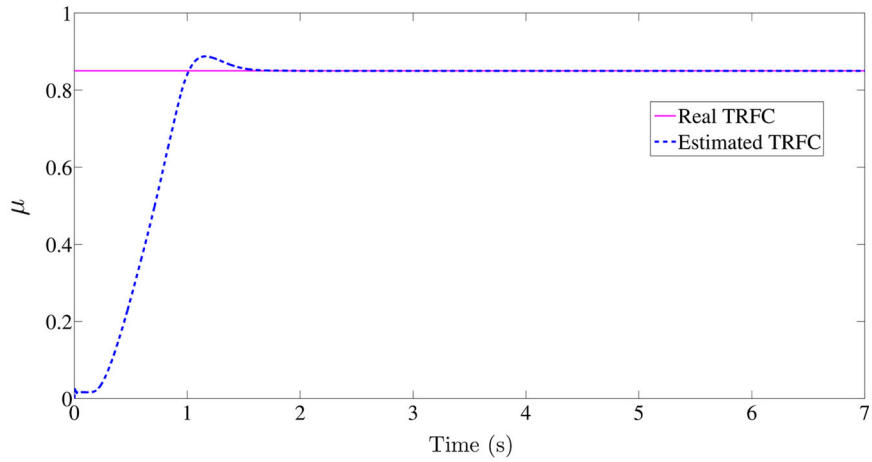

(c) TRFC estimation

In the same way, the following inequality can be obtained:

$$\begin{aligned}
&\tilde{x}_2 \sum_{i=1}^{4}(F_{\mathrm{yi}} - \hat{F}_{\mathrm{yi}})\cos\delta_i \\
&\le \left|\sum_{i=1}^{4}\frac{\partial F_{\mathrm{yi}}}{\partial x_1}(\overline{x}_i)\cos\delta_i\right| |\tilde{x}_1||\tilde{x}_2| \\
&\quad + \sum_{i=1}^{4}\frac{\partial F_{\mathrm{yi}}}{\partial x_2}(\overline{x}_i)\cos\delta_i\tilde{x}_2^2 \\
&\quad + \left|\sum_{i=1}^{4}\frac{\partial F_{\mathrm{yi}}}{\partial x_3}(\overline{x}_i)\cos\delta_i\right| |\tilde{x}_2||\tilde{x}_3|.
\end{aligned} \tag{43}$$

Therefore, (39) can be obtained. □

Theorem 2 *The states estimation $\hat{x}$ of the velocity and TRFC observer converges to the real states and the system is ISS if the observer gains l_1, l_2 and l_3 are chosen such that:*

$$\begin{aligned}
&\alpha = \frac{3\beta c_3}{\beta c_2 + 2c_1^2} \\
&\beta c_2 - \frac{1}{4}c_1^2 > 0
\end{aligned} \tag{44}$$

in which $\alpha = \frac{l_3}{l_2}$, $\beta = \frac{l_1}{l_2}$.

Proof The Lyapunov function $V(t) \in \mathcal{R}$ for the velocity and TRFC observer is defined below:

$$V(t) = \frac{1}{2}\tilde{x}_1^2 + \frac{1}{2}\tilde{x}_2^2 + \frac{1}{2}\tilde{x}_3^2. \tag{45}$$

After substituting from (32), the time derivative of (45) can be described by the following ones:

$$\begin{aligned}
\dot{V} &= \tilde{x}_1\dot{\tilde{x}}_1 + \tilde{x}_2\dot{\tilde{x}}_2 + \tilde{x}_3\dot{\tilde{x}}_3 \\
&= -l_1\tilde{x}_1^2 + l_2\tilde{x}_2\sum_{i=1}^{4}(F_{\mathrm{yi}} - \hat{F}_{\mathrm{yi}})\cos\delta_i \\
&\quad - l_3\tilde{x}_3\sum_{i=1}^{4}(F_{\mathrm{yi}} - \hat{F}_{\mathrm{yi}})\cos\delta_i \\
&\quad + (\tilde{x}_1u_1 + \tilde{x}_2u_2 + \tilde{x}_3u_3).
\end{aligned} \tag{46}$$

Based on Lemma 2, it can be shown that:

$$\begin{aligned}
\dot{V} &\le -|\tilde{x}|^T Q|\tilde{x}| + (|\tilde{x}_1|u_1 + |\tilde{x}_2|u_2 + |\tilde{x}_3|u_3) \\
&\le -|\tilde{x}|^T Q|\tilde{x}| + ||\tilde{x}|| \cdot ||u_{\mathrm{obs}}||
\end{aligned} \tag{47}$$

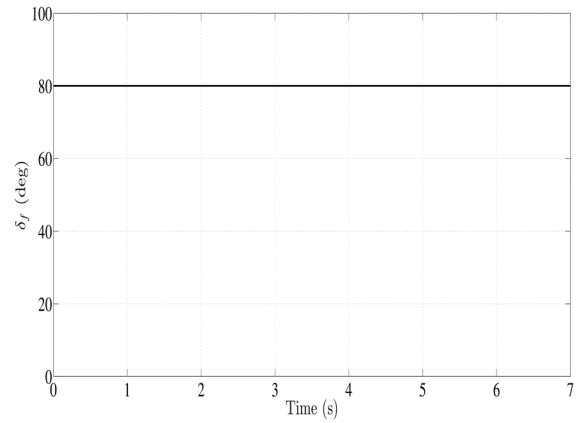

Fig. 8 Front wheel steering angle on a high-μ case

where $|\tilde{x}| \triangleq [|\tilde{x}_1|, |\tilde{x}_2|, |\tilde{x}_3|]^T$, with

$$Q = \begin{bmatrix} l_1 & -\frac{l_2c_1}{2} & \frac{l_3c_1}{2} \\ -\frac{l_2c_1}{2} & l_2c_2 & \frac{l_3c_2 - l_2c_3}{2} \\ \frac{l_3c_1}{2} & \frac{l_3c_2 - l_2c_3}{2} & l_3c_3 \end{bmatrix}.$$

Let $\alpha = \frac{l_3}{l_2}$ and $\beta = \frac{l_1}{l_2}$, then Q can be rewritten as $Q = l_2\overline{Q}$, where $\overline{Q}$ is defined as

$$\overline{Q} \triangleq \begin{bmatrix} \beta & -\frac{c_1}{2} & \frac{\alpha c_1}{2} \\ -\frac{c_1}{2} & c_2 & \frac{\alpha c_2 - c_3}{2} \\ \frac{\alpha c_1}{2} & \frac{\alpha c_2 - c_3}{2} & \alpha c_3 \end{bmatrix}. \tag{48}$$

When α is chosen such that $\alpha = \frac{3\beta c_3}{\beta c_2 + 2c_1^2}$, then the leading principal minors of $\overline{Q}$ can be calculated as follows:

$$\begin{aligned}
&D_1 = \beta, \quad D_2 = \beta c_2 - \frac{1}{4}c_1^2, \\
&D_3 = \frac{2\beta c_3^2}{\beta c_2 + 2c_1^2}\left(\beta c_2 - \frac{1}{4}c_1^2\right).
\end{aligned} \tag{49}$$

Therefore, as long as β is chosen such that $\beta c_2 - \frac{1}{4}c_1^2 > 0$, then D_1, D_2 and $D_3 > 0$ can be satisfied simultaneously. And as a result of that, $\overline{Q}$ is positive definite. Thus, there exists $|\tilde{x}|^T\overline{Q}|\tilde{x}| \ge \lambda_{\min}(\overline{Q})||\tilde{x}||^2$ and it can be derived that:

$$\dot{V} \le -l_2\lambda_{\min}(\overline{Q})||\tilde{x}||^2 + ||\tilde{x}|| \cdot ||u_{\mathrm{obs}}|| \tag{50}$$

where $\lambda_{\min}(\overline{Q})$ refers to the smallest eigenvalue of $\overline{Q}$. If l_2 is chosen such that $l_2 > \frac{\kappa}{\lambda_{\min}(\overline{Q})}$ where κ is a positive

Fig. 9 Longitudinal tire forces estimation on a high-μ case

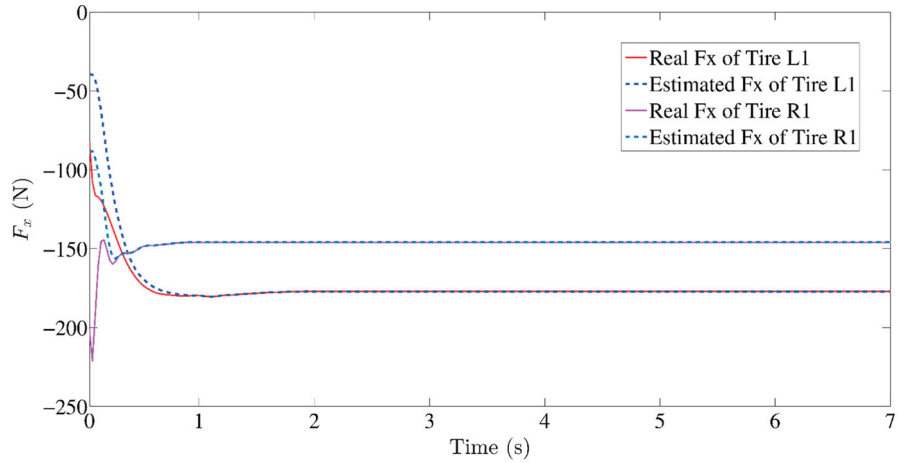

(a) Estimated errors of the front tire longitudinal forces

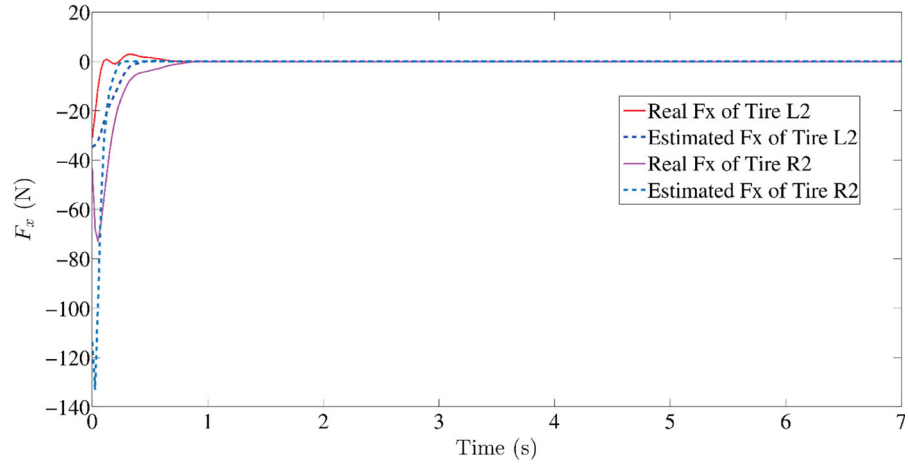

(b) Estimated errors of the rear tire longitudinal forces

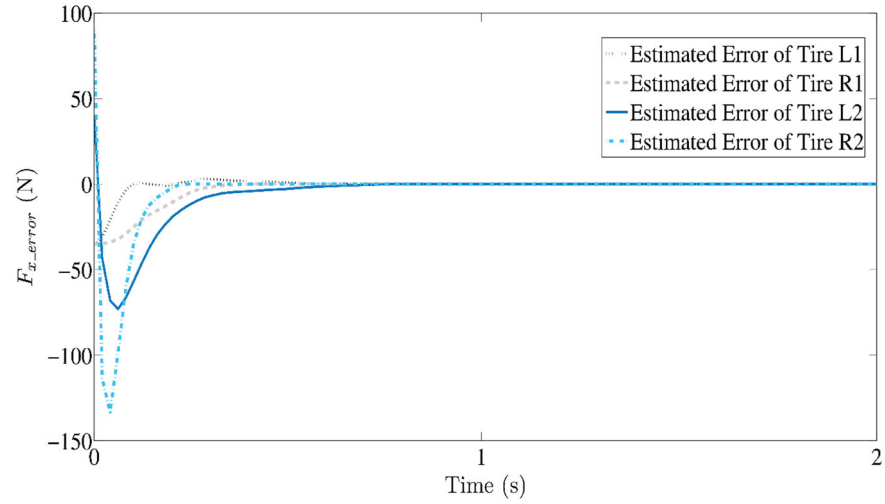

(c) Estimated errors of the longitudinal forces

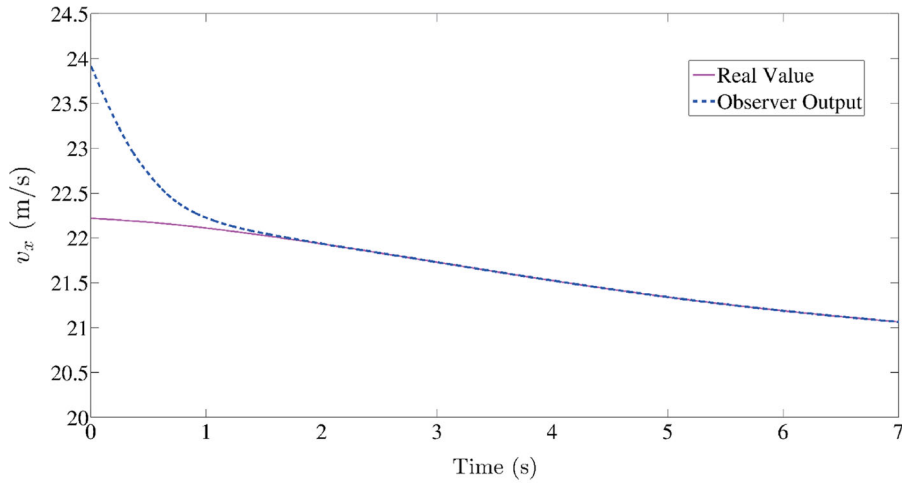

(a) Longitudinal velocity estimation

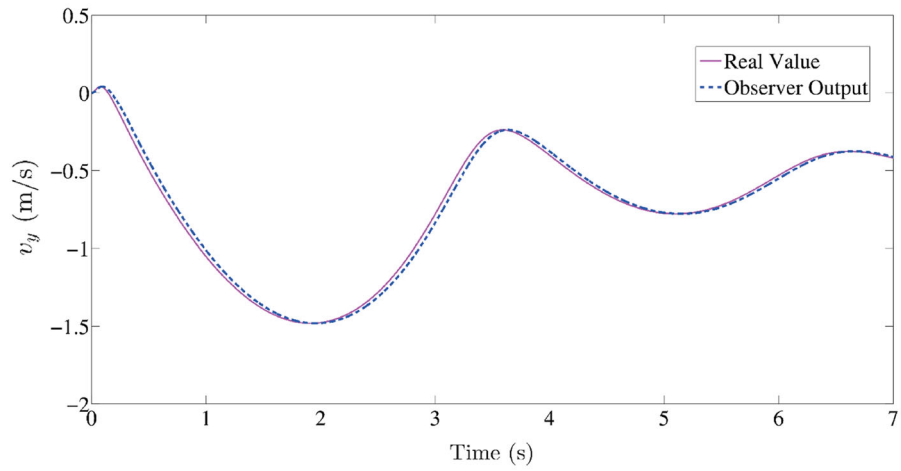

(b) Lateral velocity estimation

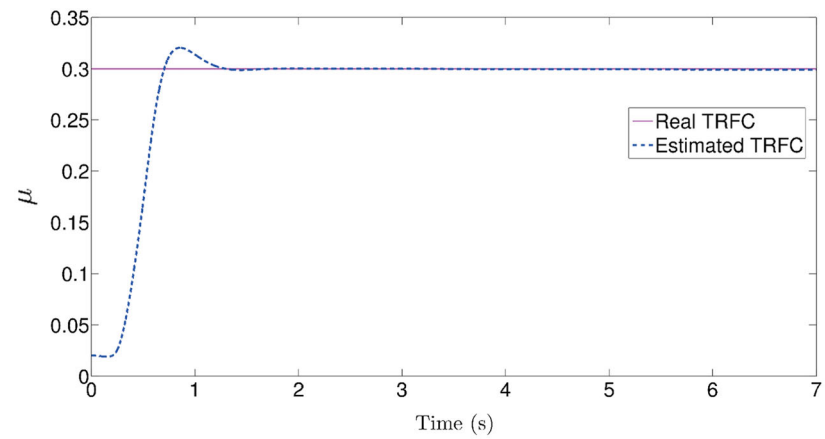

(c) TRFC estimation

Fig. 10 States estimation on a high-μ case with a large steering wheel angle

constant, $\dot{V}$ can be further constrained as follows:

$$\begin{aligned}\dot{V} &< -\kappa||\tilde{x}||^2 + ||\tilde{x}|| \cdot ||u_{\text{obs}}|| \\ &= -\kappa(\tilde{x}_1^2 + \tilde{x}_2^2 + \tilde{x}_3^2) + ||\tilde{x}|| \cdot ||u_{\text{obs}}|| \\ &= -W_2(\tilde{x}) - \theta\kappa||\tilde{x}||^2 + ||\tilde{x}|| \cdot ||u_{\text{obs}}||\end{aligned} \tag{51}$$

where $-W_2(\tilde{x}) \triangleq -\kappa(1-\theta)(\tilde{x}_1^2 + \tilde{x}_2^2 + \tilde{x}_3^2)$ and θ is a constant that can be chosen arbitrarily as long as $0 < \theta < 1$ is satisfied. Then, for all $||\tilde{x}|| \geq \frac{||u_{\text{obs}}||}{\theta\kappa}$, it can be derived that:

$$\dot{V} < -W_2(\tilde{x}) - ||\tilde{x}|| \cdot (\theta\kappa||\tilde{x}|| - ||u_{\text{obs}}||) < 0. \tag{52}$$

Therefore, according to the Theorem 4.19 described in [35], the designed observer is ISS. □

5 Simulation results

In this section, simulation results are presented to evaluate the effectiveness of the proposed method based on CarSim [36]. The vehicle model used for simulation is a rear-driven B-class hatchback. The vehicle states provided by CarSim are used as ground truth for the effectiveness verification of the designed modular observer. Parameters for the used vehicle model are based on the basic information of the B-class Hatchback vehicle type listed in the CarSim database. The detailed values are listed in Table 1.

In real driving scenarios, tire-road friction conditions are affected by several factors such as weather and the surface materials of the road, etc. On sunny days, for example, the TRFC is quite large which can be up to $\mu = 0.85$ in general. However, for the same road segment, the TRFC may drop to $\mu = 0.3$ on a snowy day. These typical driving situations are simulated to validate the performance of the designed observer system in the following subsections. Considering that white noises cannot be ignored for obtaining signal information in real driving process, states estimation with white noises are also designed.

5.1 Velocity and TRFC estimation on a high-μ case with a small steering wheel angle

The TRFC is set to $\mu = 0.85$ and as shown in Fig. 5, the command steering wheel angle is set to 30°.

Simulation results for the fixed small steering wheel angle test at a vehicle speed of 80 km/h are illustrated in Figs. 6 and 7. Both the longitudinal velocity and lateral velocity estimated from the observer follow the trend of real velocities well and it takes about 3 s for the estimated TRFC to converge to the real value. The performance of the estimation is quite accurate and the converge rate is applicable in real driving process.

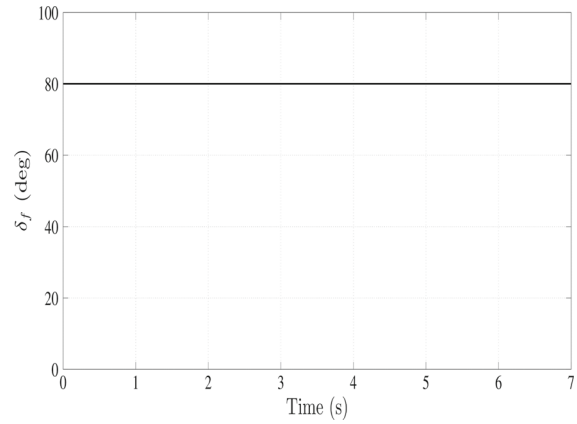

Fig. 11 Front wheel steering angle on a low-μ case

5.2 Velocity and TRFC estimation on a high-μ case with a large steering wheel angle

This is a high-μ test which simulates the dry concrete road. The TRFC is set to $\mu = 0.85$, and as shown in Fig. 8, the steering wheel angle is set to 80° which is much larger than the one in the first test.

Simulation results for the fixed large steering wheel angle test at a vehicle speed of 80 km/h is illustrated in Figs. 9 and 10. Both the longitudinal velocity and lateral velocity estimated from the observer follow the trend of real velocities well and it takes about 2 s for the estimated TRFC to converge to the real value. Compared with the small steering angle test in Sect. 5.1, it shows that the designed observer has a better performance when the steering wheel angle becomes larger.

5.3 Velocity and TRFC estimation on a low-μ case with a large steering wheel angle

The TRFC is set to $\mu = 0.3$ and as shown in Fig. 11, the command steering wheel angle is set to 80°.

Simulation results for the fixed large steering wheel angle test at a vehicle speed of 90 km/h are shown

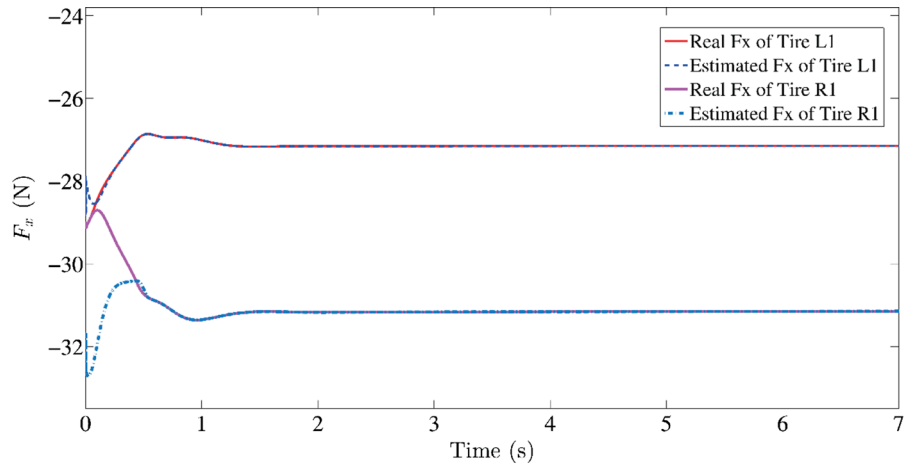

(a) Estimated errors of the front tire longitudinal forces

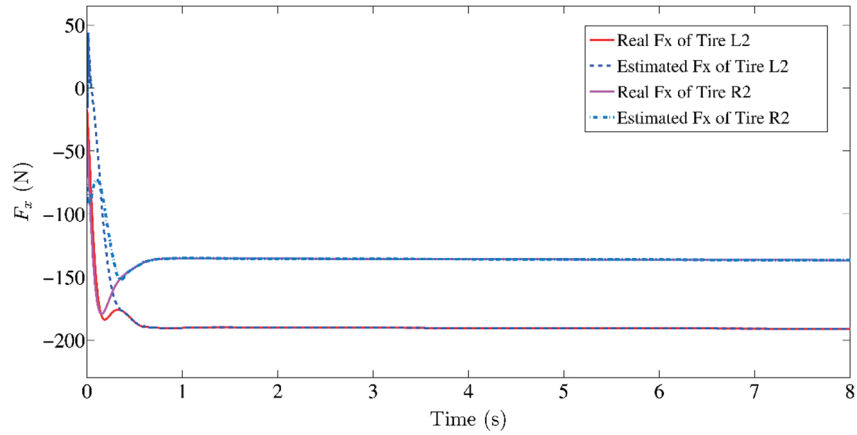

(b) Estimated errors of the rear tire longitudinal forces

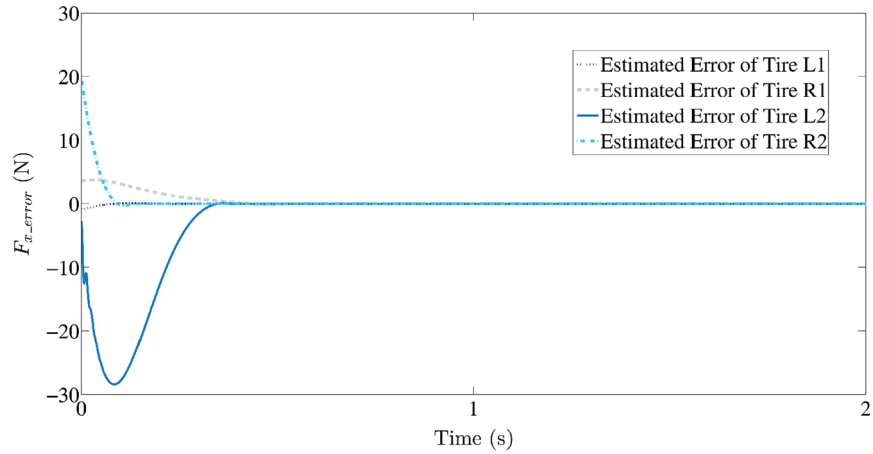

(c) Estimated errors of the longitudinal forces

Fig. 12 Longitudinal tire forces estimation on a low-μ case

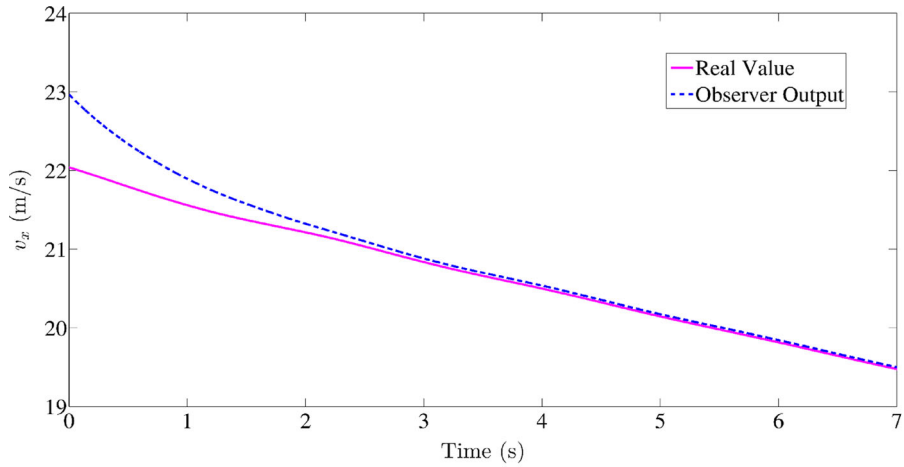

(a) Longitudinal velocity estimation

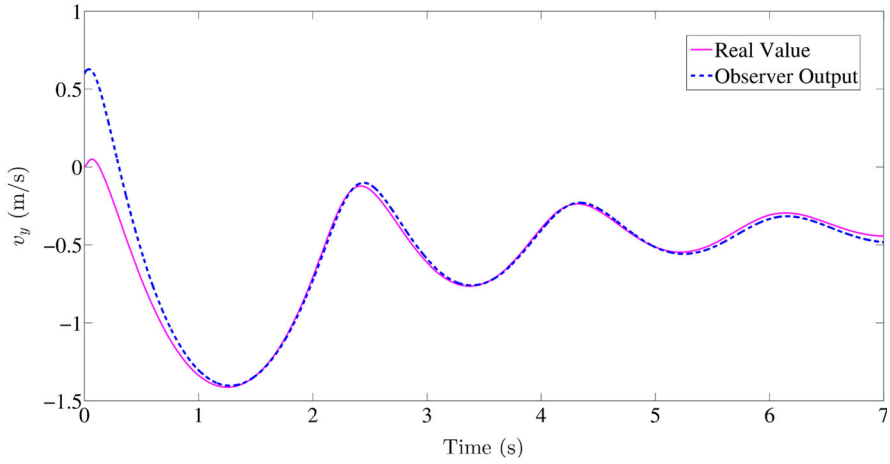

(b) Lateral velocity estimation

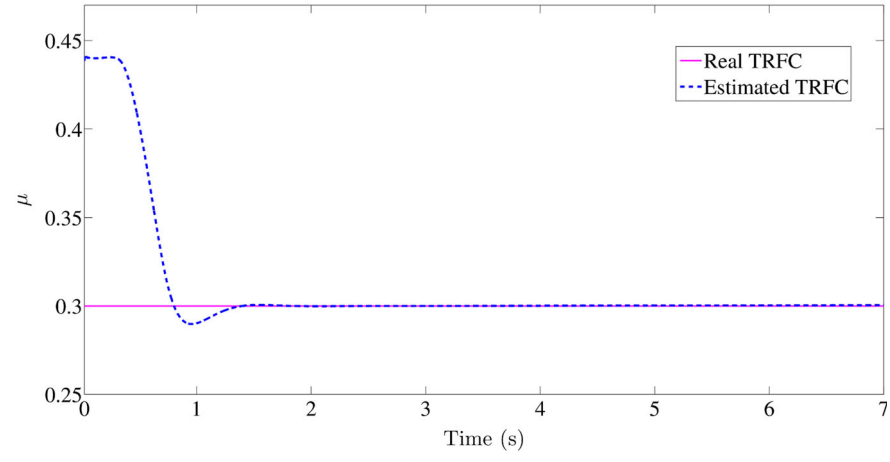

(c) TRFC estimation

Fig. 13 States estimation on a low-μ case with a large steering wheel angle

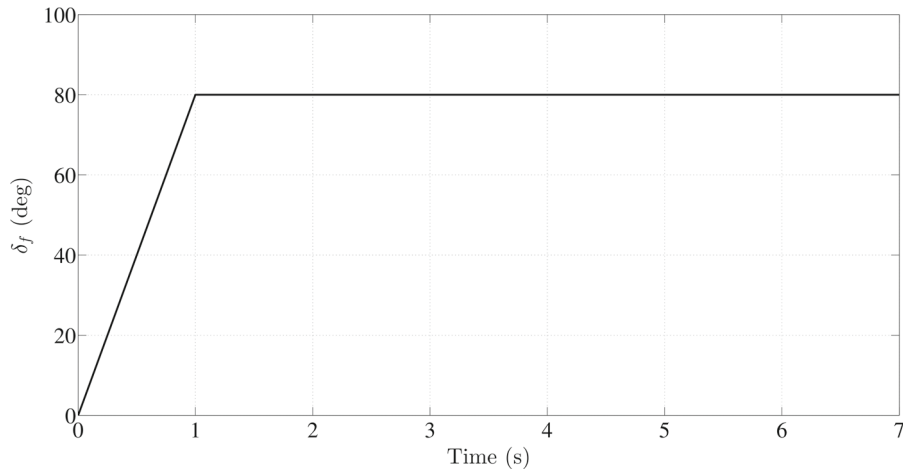

Fig. 14 Front wheel steering angle under a J-turn maneuver

in Figs. 12 and 13. In this condition, both the longitudinal velocity and lateral velocity can be estimated accurately within a quite short time which illustrates the effectiveness of the proposed method.

5.4 Velocity and TRFC estimation on a high-μ case under a J-turn situation

The J-turn condition simulates a severe and rapid change of the steer angle during the driving process. In this maneuver, the vehicle moves on a straight line in the beginning. Because the front wheel steering angle δ_f is commonly proportional to the steering wheel angle controlled by driver, δ_f is treated as the input signal. As shown in Fig. 14, at $t = 0s$, the driver turns the steering wheel from 0° to 80° within 1 s and then keeps 80° unchanged. The TRFC is set to $\mu = 0.85$ and the initial velocity is set to 80 km/h.

Both the vehicle longitudinal velocity and lateral velocity are estimated with high precision according to the simulation results presented in Fig. 15a, b. The estimated TRFC, as shown in Fig. 15c, reaches the typical high-μ value of 0.85 within 3 s after the beginning of the steering signal. Again, even at a J-turn driving condition as shown in Fig. 16, the system can still estimate the TRFC together with vehicle velocity reliably, which is acceptable in real driving process.

5.5 Velocity and TRFC estimation with white noises

In order to reflect the real driving scenarios realistically, white noises are utilized in the simulated measurements, including vehicle longitudinal and lateral acceleration rates a_x, a_y and wheel angular velocity w_i. The peak value of the white noises is set as 3% of the measurements value.

For the simulation results shown in Figs. 17, 18, 19 and 20, the vehicle velocities and TRFC can still estimate the vehicle states reliably in the presence of white noises.

6 Discussion

This paper focuses on the real-time estimation of the vehicle velocity and tire-road friction coefficient. As proposed in the Introduction, many vehicle control systems, especially active safety control systems such as ABS, traction control, vehicle stability control, collision warning, collision avoidance, adaptive cruise control (ACC), can greatly benefit from being made road-adaptive and states-known. The control algorithms can be modified to account for the external road conditions if the actual tire-road friction coefficient and vehicle velocity information are available in real time. For example, in an ACC system, speed information is the basis of algorithm implementation, and road condition information from friction coefficient estimation can be used to adjust the longitudinal spacing headway from the preceding vehicle. In the case of vehicle stability control systems, the values of vehicle velocity and tire-road friction coefficient are needed for estimating the target value of yaw rate for the vehicle. The estimation of velocity and tire-road friction coefficient is also useful for winter maintenance vehicles like snowplows.

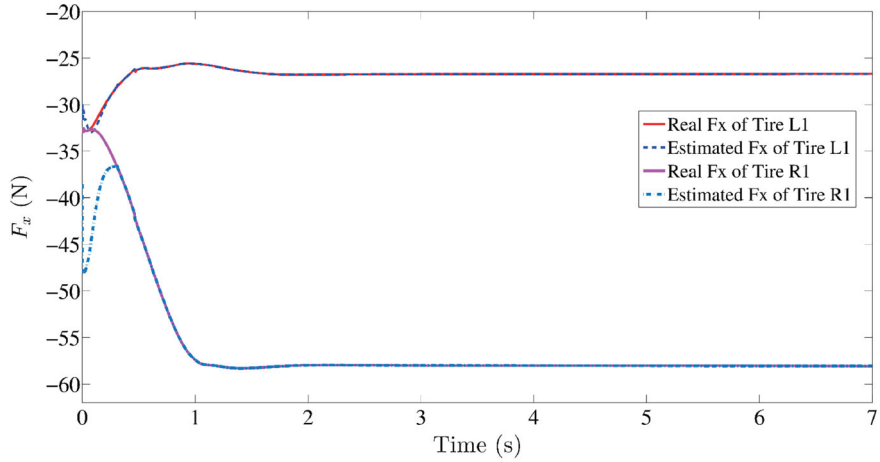

(a) Estimated errors of the front tire longitudinal forces

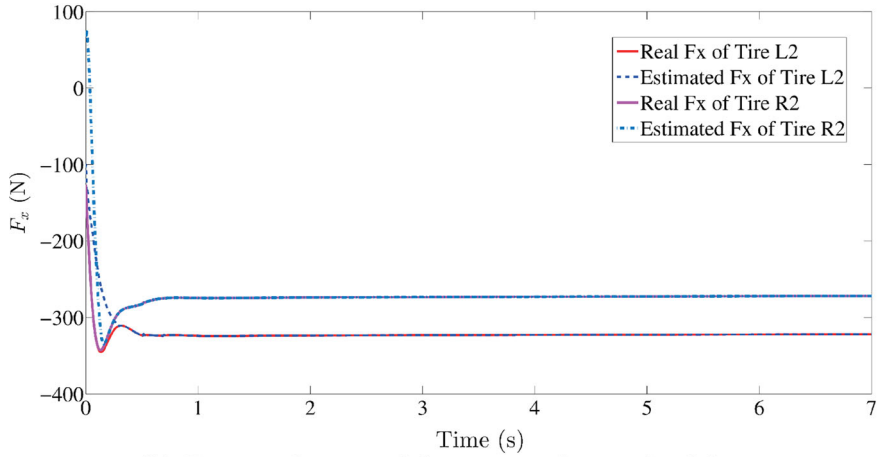

(b) Estimated errors of the rear tire longitudinal forces

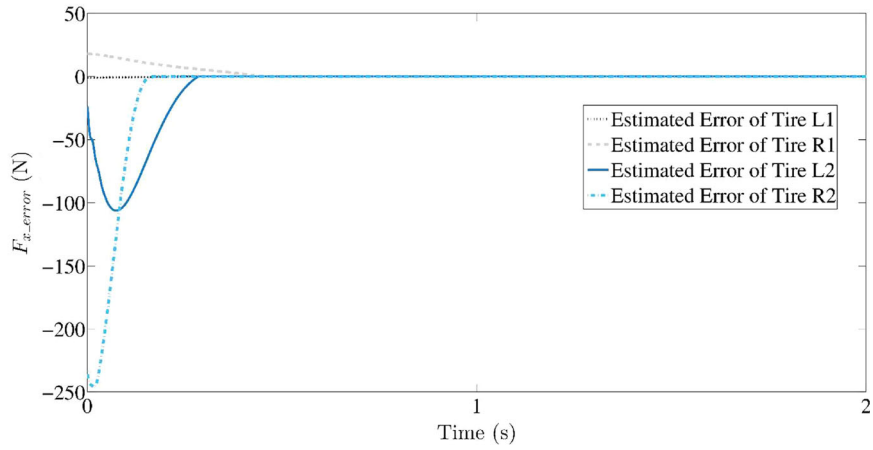

(c) Estimated errors of the longitudinal forces

Fig. 15 Longitudinal tire forces estimation on a high-μ case under a J-turn

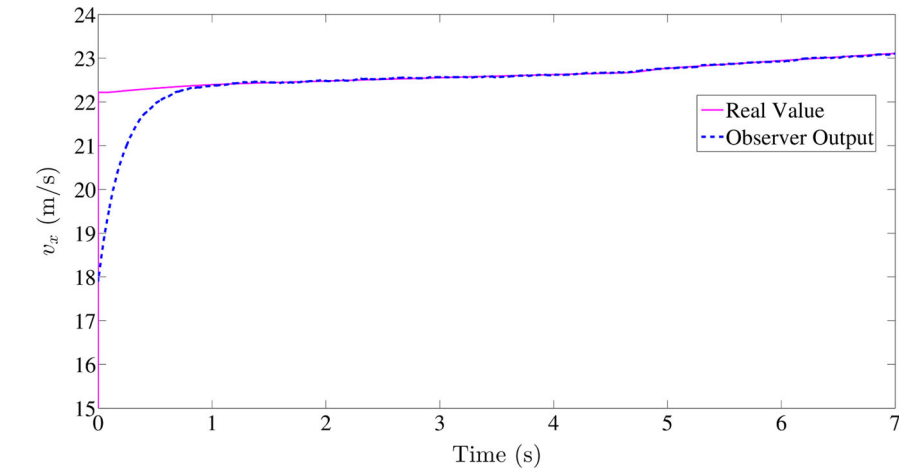

(a) Longitudinal velocity estimation

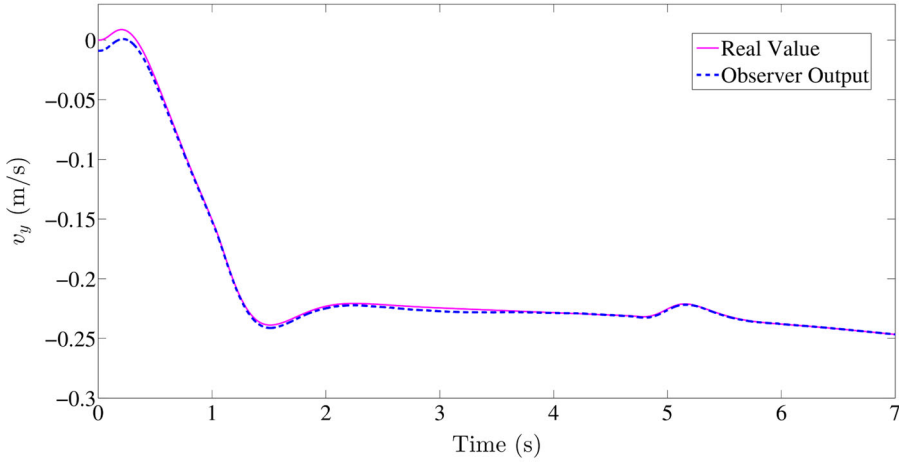

(b) Lateral velocity estimation

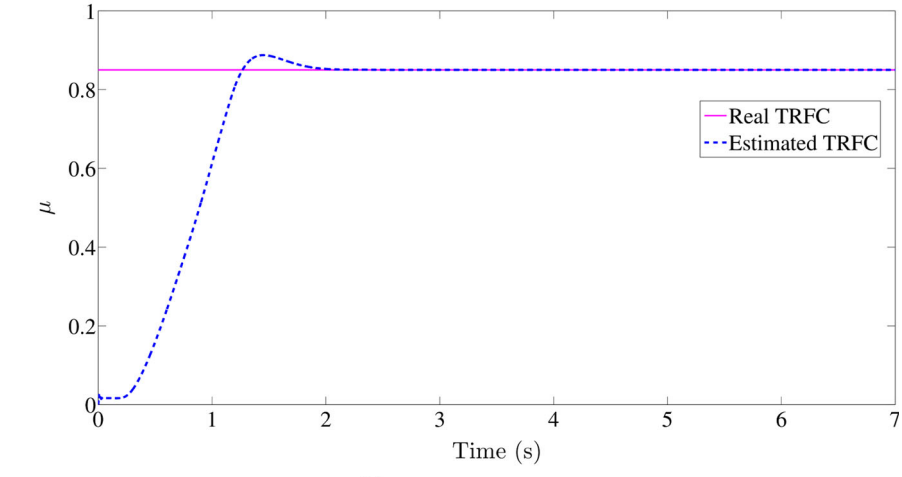

(c) TRFC estimation

Fig. 16 States estimation on a high-μ case under a J-turn maneuver

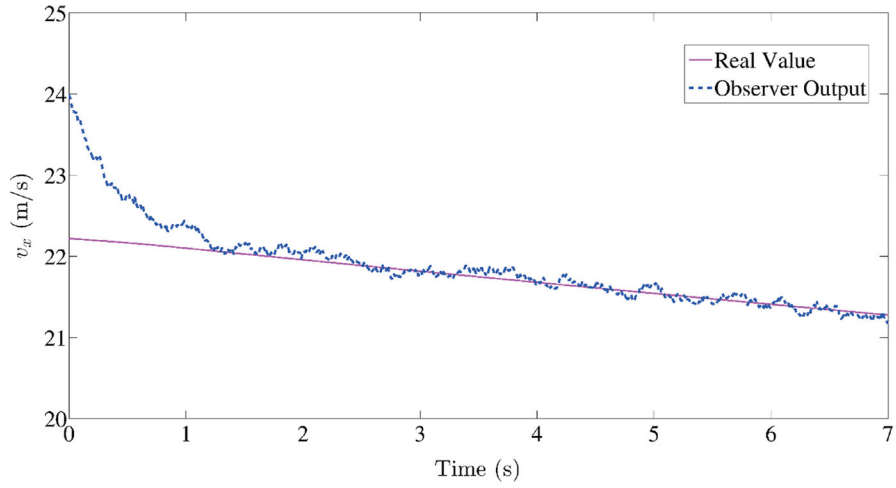

(a) Longitudinal velocity estimation

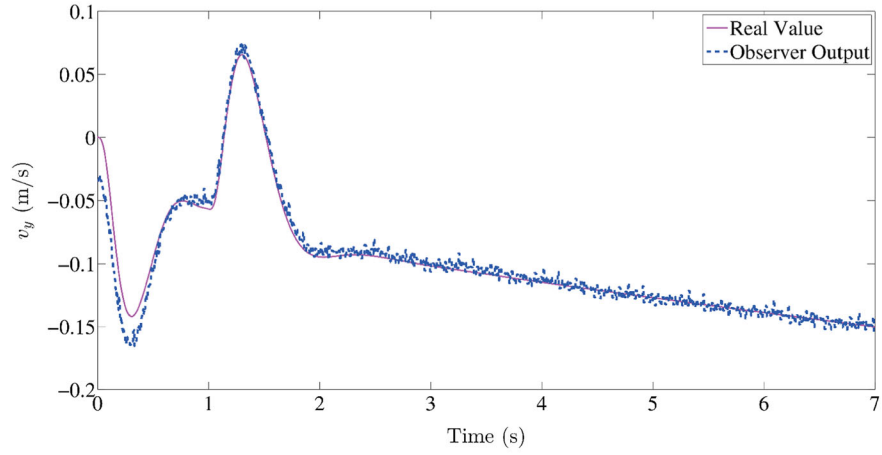

(b) Lateral velocity estimation

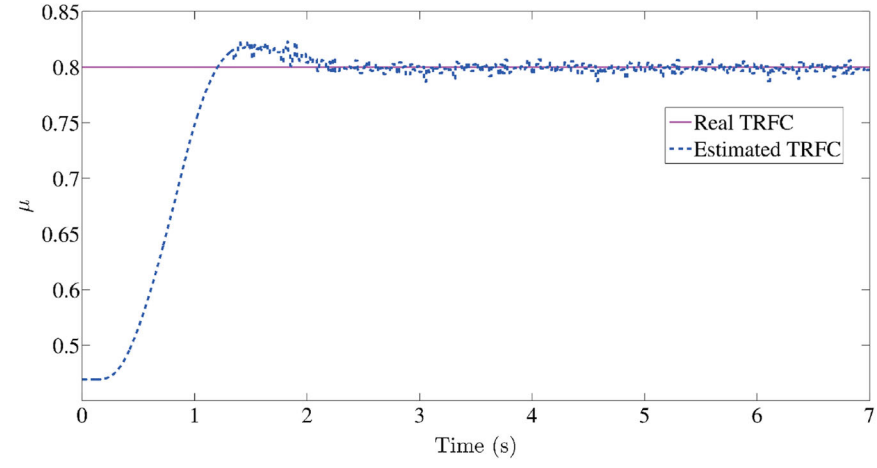

(c) TRFC estimation

Fig. 17 Noises test on a high-μ case with a small steering wheel angle

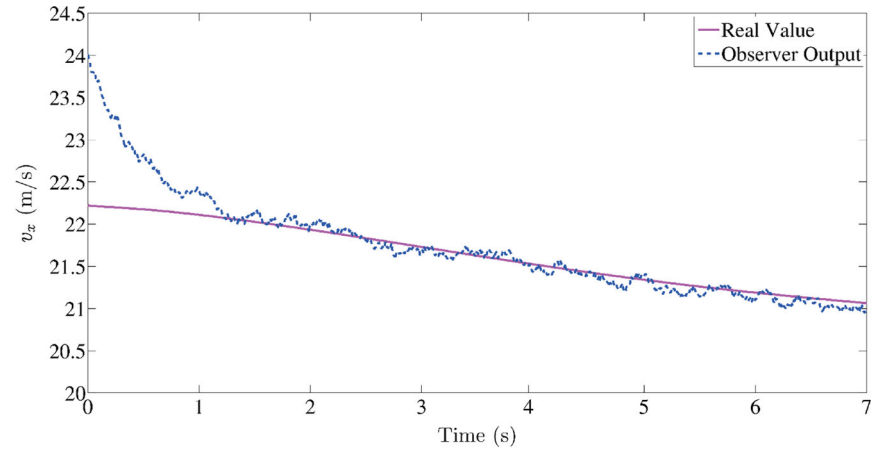

(a) Longitudinal velocity estimation

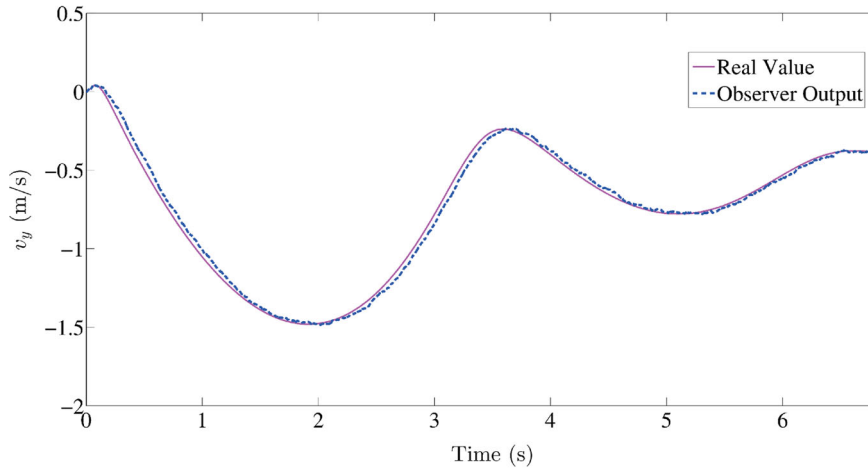

(b) Lateral velocity estimation

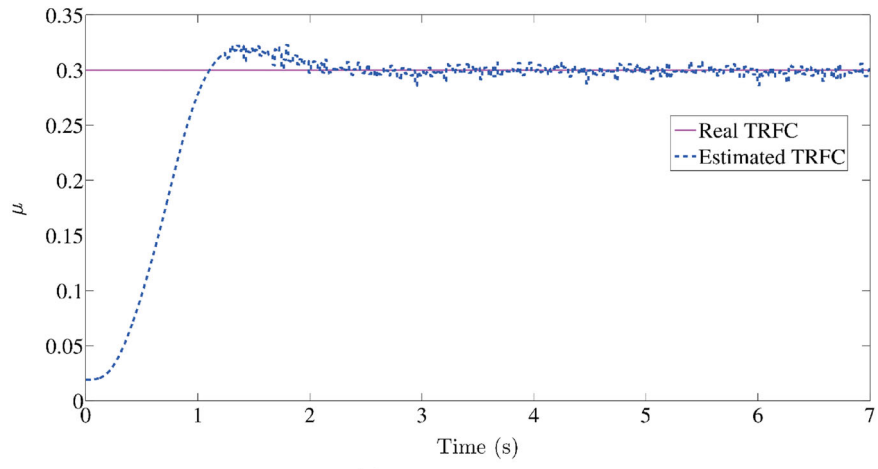

(c) TRFC estimation

Fig. 18 Noises test on a high-μ case with a large steering wheel angle

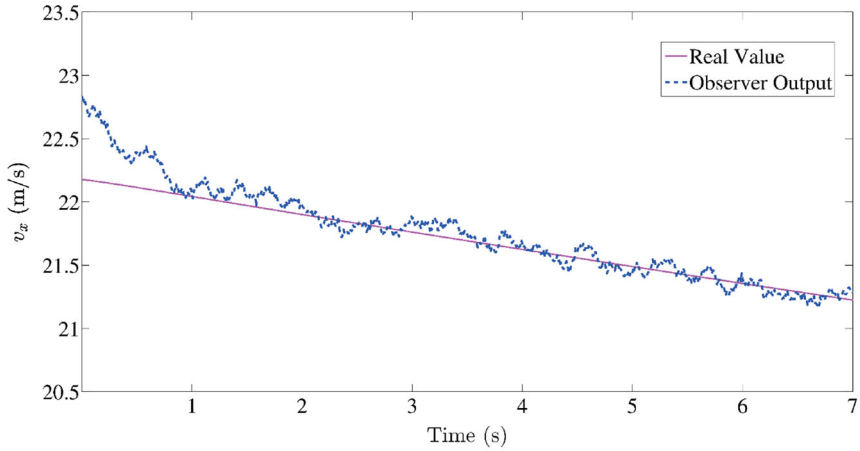

(a) Longitudinal velocity estimation

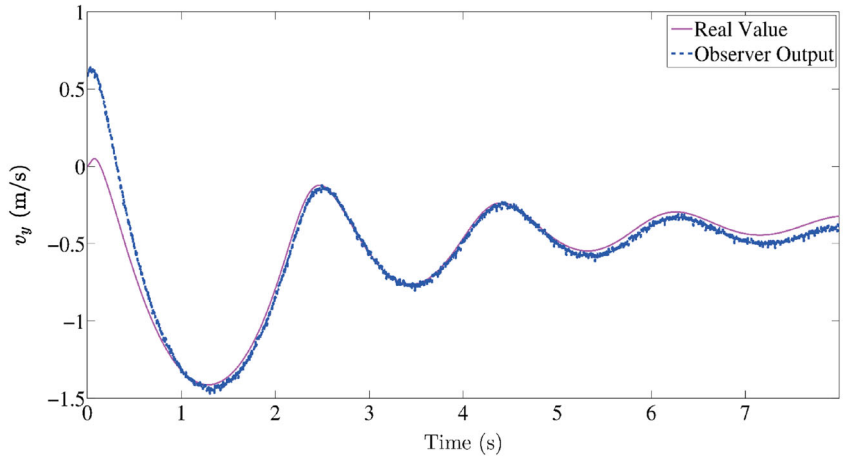

(b) Lateral velocity estimation

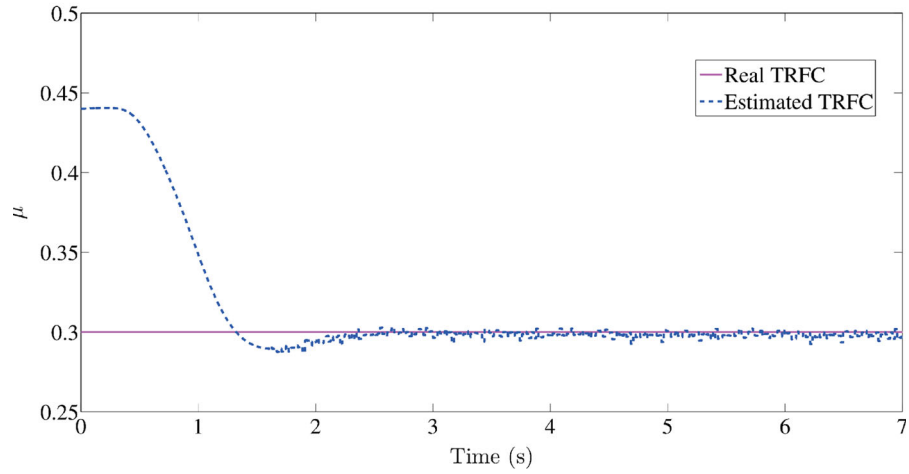

(c) TRFC estimation

Fig. 19 Noises test on a low-μ case with a large steering wheel angle

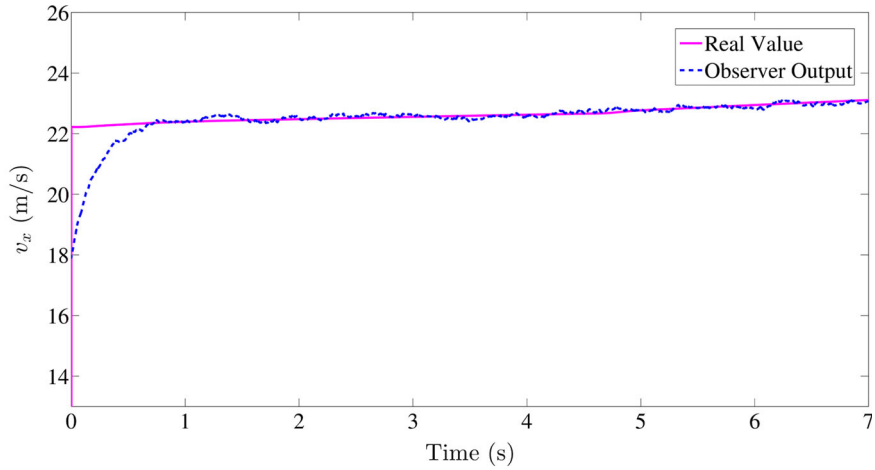

(a) Longitudinal velocity estimation

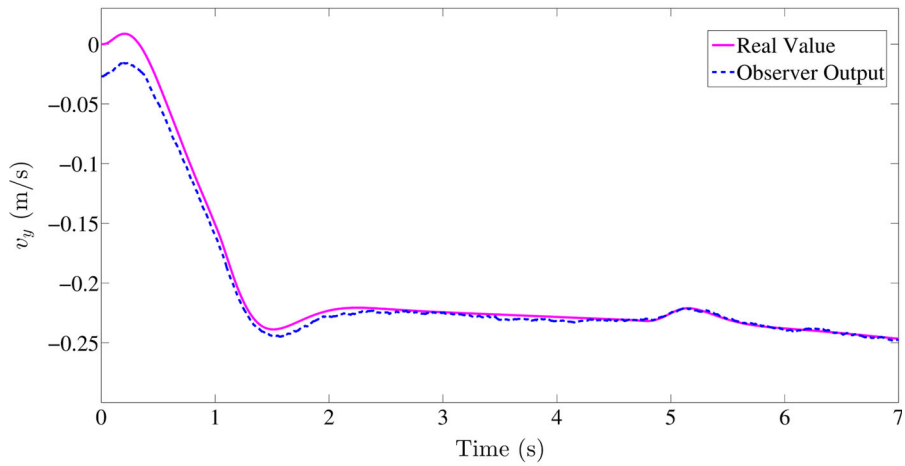

(b) Lateral velocity estimation

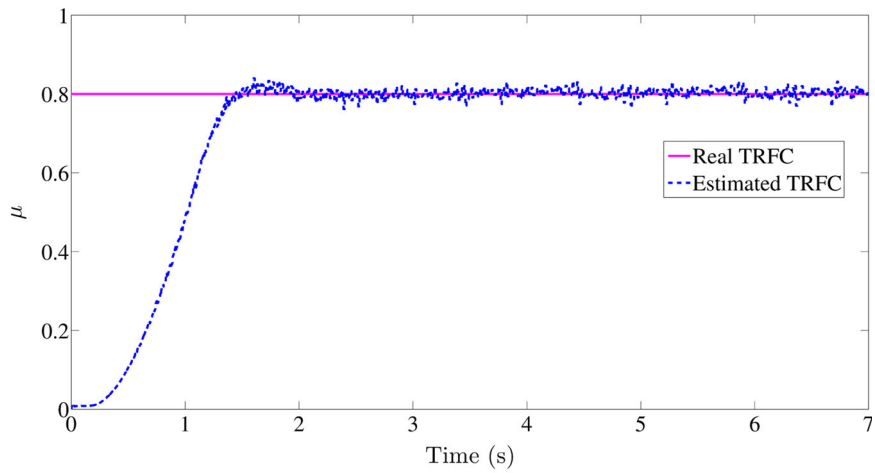

(c) TRFC estimation

Fig. 20 Noises test on a high-μ case under a J-turn maneuver

For such vehicles that have to operate in a harsh winter road environment, the knowledge of velocity and friction coefficient can help to improve the safety of operation. Furthermore, the vehicle operator can use these information to adjust the amount and kind of deicing material to be applied to the roadway. It can also be used to automate the application of deicing material.

Direct estimation methods using sensors such as differential GPS and accelerometers have different limitations. Limitations of utilizing differential GPS include the slow update rates and the lack of wide availability of differential correction. Limitations involved with using an accelerometer to estimate vehicle velocity include its sensitivity to vertical vibrations as well as road grade inputs and bias errors. The proposed method in this paper can avoid these problems effectively. However, a limitation of the developed system is that it requires sufficient road grade information in order to estimate the friction coefficient accurately. Estimating the information of the road grade and the bank angle accurately is still one of the future research directions.

7 Conclusions

In this paper, a new velocity and TRFC estimation method for a vehicle system is proposed based on the wheel angular velocity filter observer and the lateral tire friction model. The proposed observer system is demonstrated to be input-to-state stable based on a complete stability analysis using Lyapunov-based methods. In comparison with existing works on vehicle state estimation, the contribution of the proposed method is the simultaneous estimation of vehicle velocities and the identification of the TRFC for different road surface conditions. Simulation results are presented to demonstrate the effectiveness of the proposed estimation method.

References

1. Hu, H., Wu, Z.: Stability and hopf bifurcation of four-wheel-steering vehicles involving driver's delay. Nonlinear Dyn. **22**(4), 361–374 (2000)
2. Zhang, X., Xu, Y., Pan, M.: A vehicle ABS adaptive sliding-mode control algorithm based on the vehicle velocity estimation and tyre-road friction coefficient estimation. Veh. Syst. Dyn. **52**(4), 475–503 (2014)
3. Rossa, F.D., Mastinu, G.: Analysis of the lateral dynamics of a vehicle and driver model running straight ahead. Nonlinear Dyn. **92**(7–8), 1–10 (2017)
4. Chen, J., Yu, J., Zhang, K., Ma, Y.: Control of regenerative braking systems for four-wheel-independently-actuated electric vehicles. Mechatronics **50**, 394–401 (2018)
5. Li, B., Du, H., Li, W.: A novel cost effective method for vehicle tire-road friction coefficient estimation. In: Proceeding of IEEE/ASME International Conference on Advanced Intelligent Mechatronics, pp. 1528–1533 (2013)
6. Ahn, C., Peng, H., Tseng, H.E.: Robust estimation of road frictional coefficient. IEEE Trans. Control Syst. Technol. **21**(1), 1–13 (2013)
7. Lee, C., Hedrick, K., Yi, K.: Real-time slip-based estimation of maximum tire-road friction coefficient. IEEE-ASME Trans. Mechatron. **9**(2), 454–458 (2004)
8. Eichhorn, U., Roth, J.: Prediction and monitoring of tyre-road friction. In: Proceeding of Fisita, London, pp. 7–11 (1992)
9. Braghin, F., Brusarosco, M., Cheli, F.: Measurement of contact forces and patch features by means of accelerometers fixed inside the tire to improve future car active control. Veh. Syst. Dyn. **44**(1), 3–13 (2006)
10. Pasterkamp, W.R., Pacejka, H.B.: The tyre as sensor to estimate friction. Veh. Syst. Dyn. **27**(5), 409–422 (2007)
11. Tanelli, M., Piroddi, L., Savaresi, S.M.: Real-time identification of tire-road friction conditions. IET Control Theory A **3**(7), 891–906 (2009)
12. Yu, H., Taheri, S., Duan, J.: An integrated cooperative antilock braking control of regenerative and mechanical system for a hybrid electric vehicle based on intelligent tire. Asian J. Control **18**(1), 55–68 (2016)
13. Wang, J., Alexander, L., Rajamani, R.: Friction estimation on highway vehicles using longitudinal measurements. J. Dyn. Syst. Meas. Control **126**(2), 265–275 (2004)
14. Kim, T., Lee, J., Yi, K.: Enhanced maximum tire-road friction coefficient estimation based advanced emergency braking algorithm. In: Proceeding of 2015 IEEE Intelligent Vehicles Symposium (IV), Seoul, pp. 883–888 (2015)
15. Wang, R., Wang, J.: Tire-road friction coefficient and tire cornering stiffness estimation based on longitudinal tire force difference generation. Control Eng. Pract. **21**(1), 65–75 (2013)
16. Nakakuki, T., Shen, T., Tamura, K.: Adaptive control approach to uncertain longitudinal tire slip in traction control of vehicles. Asian J. Control **10**(1), 67–73 (2010)
17. Rajamani, R., Piyabongkarn, D., Lew, J. Grogg, J.: Algorithms for real-time estimation of individual wheel tire-road friction coefficients. In: Proceeding of American Control Conference (ACC), Minneapolis, MN, pp. 6–11 (2006)
18. Wang, R., Yin, G., Wang, J.: Vehicle lateral velocity and tire-road friction coefficient estimation. In: Proceeding of Dynamic Systems and Control Conference Joint with the JSME, Motion and Vibration Conference, pp. 495–502 (2012)
19. Tanelli, M., Ferrara, A., Giani, P.: Combined vehicle velocity and tire-road friction estimation via sliding node observers. In: Proceeding of 2012 IEEE International Conference on Control Applications, Dubrovnik, pp. 130–135 (2012)
20. Yu, J., Chen, J., Peng, Y., Liu, H.: Nonlinear observer for longitudinal and lateral velocities of vehicles based on the esti-

mation of longitudinal tire forces. In: Proceeding of American Control Conference (ACC), Boston, MA, pp. 6887–6892 (2016)
21. Kim, S., Kim, H.: Systematic robustness analysis of least squares mobile robot velocity estimation using a regular polygonal optical mouse array. Asian J. Control **14**(2), 348–358 (2012)
22. Zhao, L.H., Liu, Z.Y., Chen, H.: Design of a nonlinear observer for vehicle velocity estimation and experiments. IEEE Trans. Control Syst. Technol. **19**(3), 664–672 (2011)
23. Li, L., Song, J., Kong, L.: Vehicle velocity estimation for real-time dynamic stability control. Int. J. Automot. Technol. **10**(6), 675–685 (2009)
24. Guo, H., Chen, H., Xu, F., Wang, F., Lu, G.: Implementation of EKF for vehicle velocities estimation on FPGA. IEEE Trans. Ind. Electron. **60**(9), 3823–3835 (2013)
25. Huang, X., Wang, J.: Real-time estimation of center of gravity position for lightweight vehicles using combined AKF–EKF method. IEEE Trans. Veh. Technol. **63**(9), 4221–4231 (2014)
26. Xin, Q., Shi, Z.: Robust adaptive backstepping controller design for aircraft autonomous short landing in the presence of uncertain aerodynamics. J. Aerosp. Eng. **31**(2), 04018005 (2018)
27. Xin, Q., Shi, Z.: Prediction and recovery of aircraft unstable nonlinear phenomena using bifurcation analysis and backstepping method. J. Comput. Nonlinear Dyn. **11**(6), 061007 (2016)
28. Imsland, L., Johansen, T., Fossen, T., Kalkkuhl, J., Suissa, A.: Vehicle velocity estimation using modular nonlinear observers. In: Proceedings of the 44th IEEE Conference on Decision and Control (CDC), pp. 6728–6733 (2005)
29. Rajamani, R.: Vehicle Dynamics and Control. Springer, New York (2011)
30. Imslanda, L., Johansena, T.A., Fossena, T.I., Grip, H.F., Kalkkuhlb, J.C., Suissab, J.: Vehicle velocity estimation using nonlinear observers. Automatica **42**(12), 2091–2103 (2006)
31. Sun, F., Huang, X., Rudolph, J., Lolenkod, K.: Vehicle state estimation for anti-lock control with nonlinear observer. Control Eng. Pract. **43**, 69–84 (2015)
32. Pacejka, H.: Tire and Vehicle Dynamics, 3rd edn. Butterworth-Heinemann, Waltham, MA (2012)
33. Hahn, J.O., Rajamani, R., Alexander, L.: GPS-based real-time identification of tire-road friction coefficient. IEEE Trans. Control Syst. Technol. **10**(3), 331–343 (2002)
34. She, J., Makino, K., Ouyang, L.: Estimation of normalized longitudinal force for an electric cart using equivalent-input-disturbance approach. IEEE Trans. Veh. Technol. **63**(8), 3642–3650 (2014)
35. Khalil, H.K.: Nonlinear Systems, 3rd edn. Prentice-Hall, Upper Saddle River, NJ (2002)
36. Mechanical Simulation Corporation. Ann Arbor, MI 48103, http://www.carsim.com/company/index.php (2019). Accessed 29 Jan 2019